Journal of the Meteorological Society of Japan

EARLY ONLINE RELEASE

The DOI for this manuscript is
DOI:10.2151/jmsj.2020-061
J-STAGE Advance published date: August 3rd 2020

Maintenance Mechanism of Rossby Wave Breaking and Pacific-Japan Pattern in Boreal Summer

Kazuto TAKEMURA[1]

Graduate School of Science
Kyoto University, Kyoto, Japan

Climate Prediction Division
Japan Meteorological Agency, Tokyo, Japan

and

Hitoshi MUKOUGAWA

Graduate School of Science
Kyoto University, Kyoto, Japan

----

1) Corresponding author: Kazuto Takemura, Graduate School of Science, Kyoto University, Kitashirakawa Oiwake-cho, Sakyo, Kyoto 606-8502, JAPAN.
Email: takemura.kazuto@kugi.kyoto-u.ac.jp
Tel: +81-75-xxxx-xxxx
Fax: +81-75-xxxx-xxxx

Abstract

To reveal a maintenance mechanism for Rossby wave breaking (RWB) east of Japan and Pacific-Japan (PJ) pattern, which are triggered due to quasi-stationary Rossby wave propagation along the Asian jet, the past 44 RWB cases east of Japan is analyzed using a reanalysis dataset. A comparison between the composites of 7 persistent and 7 non-persistent cases, which are classified based on duration of the RWB and the PJ pattern, indicates that the persistent case shows the stronger and longer-lived quasi-stationary Rossby wave propagation along the Asian jet. The subsequent stronger RWB in the persistent case causes the consequential formation of the more enhanced PJ pattern, through the stronger high potential vorticity intrusion toward the subtropical western North Pacific. The persistent case further shows a persistent northward tilting vertical structure of the anomalous anticyclone east of Japan, accompanied by the enhanced anomalous warm air advection in the lower to middle troposphere north of the anomalously extended North Pacific Subtropical High associated with the PJ pattern. The ***Q***-vector diagnosis and partial correlation analysis indicate that the anomalous warm air advection in the middle troposphere is closely associated with dynamically induced anomalous ascent from Japan to the east by an adiabatic process. Enhanced anomalous moisture flux convergence from Japan to the east, which is due to moisture inflow along the fringe of North Pacific Subtropical High from the subtropical western

North Pacific, also causes the anomalous ascent over the region by a diabatic process. A simple correlation analysis indicates nearly equivalent associations of the adiabatic and diabatic factors with the anomalous ascent. The anomalous ascent contributes to the enhanced and persistent RWB, through negative vorticity tendency due to vortex squashing in the upper troposphere, which further contributes to the enhanced and persistent PJ pattern in the persistent case.

Keywords North Pacific high; warm air; moist air; ascending current; wave breaking

1. Introduction

Increased socio-economic damages resulting from the unprecedented heat waves over Japan during boreal summer are attributable not only to a transient anomalous extension of the North Pacific Subtropical High (NPSH) (e.g., Lu and Dong 2001; Enomoto et al. 2003; Wakabayashi and Kawamura 2004; Liu et al. 2019) but also to its persistence (Shimpo et al. 2019). The persistent anomalous extension of the NPSH toward Japan thus is expected to contribute to significant anomalous hot summer climate over the region. In some cases, the extended NPSH causes persistent anomalous moisture inflows from the south along the southwestern to northern fringe of the enhanced anomalous anticyclonic flow (e.g., Ninomiya and Kobayashi 1999; Rodwell and Hoskins 2001; Lu 2002), contributing torrential rainfall events. The central position and persistence of the NPSH is one of the essential factors regulating the summer climate over Japan and its operational seasonal forecasting.

It has been well known that enhanced and suppressed convection over the tropical western North Pacific (WNP) east of the Philippines are closely associated with anomalous anticyclonic and cyclonic circulation over Japan in the lower troposphere, contributing to anomalous hot and cool summer conditions, respectively (e.g., Lu and Dong 2001; Nitta 1987; Wakabayashi and Kawamura 2004). The teleconnection pattern, which shows the relationship between the convective activity near the Philippines and the lower-tropospheric anomalous circulation over Japan, is referred to as the Pacific-Japan (PJ) pattern (Nitta 1987). The enhanced extension of the NPSH to mainland Japan is thus associated with the enhanced convection to the south through a formation of the PJ pattern (Kawamura et al. 1998, 2001; Wakabayashi and Kawamura 2004). Kosaka and Nakamura (2006) further elucidated northward tilting vertical structure of the PJ pattern in the troposphere. The northward tilted anomalous vorticity is consistent with zonal thermal contrast between heated Eurasian continent and relatively cool sea surface over the North Pacific in summer (Kosaka and Nakamura 2006; Xu et al. 2019).

The amplified ridge near Japan in the upper troposphere also can excite the anomalous anticyclone in the lower troposphere, corresponding to a formation mechanism of the Bonin high with the equivalent barotropic structure (Enomoto et al. 2003), which is resulting from a quasi-stationary Rossby wave propagation along the Asian jet referred to as the Silk-Road pattern (Lu et al. 2002; Enomoto et al. 2003). It is well known that the propagating wave energy frequently induces Rossby wave breaking (RWB) near the Asian jet exit region near Japan (Postel and Hitchman 1999, 2001; Abatzoglou and Magnusdottir 2006; Hitchman and Huesmann 2007; Homeyer and Bowman 2013). Recently, Takemura and Mukougawa (2020) (hereafter referred to as TM20) showed from a result of lag composite analysis that the RWB east of Japan, which is resulting from the wave propagation along the Asian jet, can excite the PJ pattern through a southwestward intrusion of high potential vorticity (PV) air mass toward the subtropical WNP, and consequently contribute to the anomalously extended NPSH to mainland Japan.

An influence of the anomalously extended NPSH associated with the PJ pattern on the anomalous anticyclone in the upper troposphere, if it exists, will be one of the remarkable processes indicating a wave source of the RWB from the lower troposphere. Pfahl et al. (2015) showed that enhancement and persistence of atmospheric blocking ridge is attributable not only to northward intrusion of low PV air mass associated with the RWB but also the upper-level low PV tendency associated with anomalous ascent from the lower troposphere and the consequent anomalous latent heating. Grams and Archambault (2016) examined an influence of recurving tropical cyclone on extratropical circulation, also indicating an importance of the anomalous ascent to an enhancement of the blocking ridge and its further downstream impacts. The contribution of the upward influence of cyclonic disturbance to the enhanced upper-level blocking ridge can be explained by negative vorticity tendency associated with the vortex squashing effect resulting from the anomalous ascent, as indicated by Wiel et al. (2015). Although these results suggest that the anomalous moisture inflow along the southwestern to northern fringe of the NPSH may contribute to the anomalous anticyclone in the upper troposphere through the anomalous ascent north of the NPSH, the associated process has not been examined as yet. The northward tilting vertical structure indicated by Kosaka and Nakamura (2006) is expected to be favorable for the aforementioned process through the north-south shift of the anomalous anticyclones between the upper and lower troposphere.

The persistent RWB accompanied by the anomalous anticyclone in the upper troposphere, which is sustained by the anomalous ascent north of the NPSH, is expected to recursively contribute to the persistent PJ pattern, indicating an existence of so-called positive feedback mechanism between the RWB and PJ pattern resulting from the process indicated by TM20. This study examines the maintenance mechanism of the RWB east of Japan and the anomalously extended NPSH associated with the PJ pattern, analyzing the past 44 RWB cases extracted in TM20. This line of investigation is important to elucidate the essential process causing the persistent anomalous summer climate and the consequent socio-economic impacts.

The structure of the present paper is organized as follows. Section 2 describes the dataset and analytical methods. In Section 3, results of the lag composite analysis for the cases classified by the duration of the RWB and the PJ pattern are provided to show a difference in the atmospheric characteristics between persistent and non-persistent cases. In Section 4, using a quasi-geostrophic diagnosis and a partial correlation analysis, we assess contribution of anomalous thermal advection along the western to northern fringe of NPSH in the middle troposphere to the extended anomalous anticyclone east of Japan in the upper troposphere. In Section 5, from a moisture flux diagnosis and a trajectory analysis, we further assess contribution of anomalous moisture convergence in the lower to middle troposphere to the extended anomalous anticyclone east of Japan. In Section 6, an influence of the anomalous ascent from Japan to the east on the enhanced and persistent anomalous anticyclone in the upper troposphere will be summarized, using a simple vorticity budget analysis, according to the results described in Sections 4 and 5. Section 7 provides the major findings of the study.

2. Data and Methods

The data used in this study are those from 6-hourly and daily mean datasets of the Japanese 55-year reanalysis (JRA-55) for June–September (JJAS) during the 61-year period from 1958 to 2018, with a horizontal resolution of 1.25° and 37 pressure levels (Kobayashi et al. 2015). We also used the daily mean dataset of COBE-SST (Ishii et al. 2005) for June–August during the 61-year period, with a resolution of 1°, to analyze sea surface temperature (SST). Here, the anomaly is defined as a departure from the climatology, which is obtained as the 60-day low-pass filtered 30-year daily averages from 1981 to 2010 using a Lanczos filter (Duchon 1979). To extract low-frequency components including the quasi-stationary Rossby wave, a 5-day-running mean is applied to the daily anomaly data. We next applied a horizontal smoothing filter to relative vorticity fields using a triangular truncation retaining N = 24 wavenumbers (T24) to exclude the disturbances at a scale smaller than synoptic eddies. Spatial partial derivative is calculated using the spherical coordinates.

The propagation of quasi-stationary Rossby wave packets is analyzed using the wave activity flux (WAF) defined by Takaya and Nakamura (2001). The horizontal WAF is defined as follows:

$$\boldsymbol{W} = \frac{\cos\phi}{2|\overline{\boldsymbol{U}}|}\begin{pmatrix} \frac{\bar{u}}{r^2\cos^2\phi}\left[\left(\frac{\partial\psi'}{\partial\lambda}\right)^2 - \psi'\frac{\partial^2\psi'}{\partial\lambda^2}\right] + \frac{\bar{v}}{r^2\cos\phi}\left[\frac{\partial\psi'}{\partial\lambda}\frac{\partial\psi'}{\partial\phi} - \psi'\frac{\partial^2\psi'}{\partial\lambda\partial\phi}\right] \\ \frac{\bar{u}}{r^2\cos\phi}\left[\frac{\partial\psi'}{\partial\lambda}\frac{\partial\psi'}{\partial\phi} - \psi'\frac{\partial^2\psi'}{\partial\lambda\partial\phi}\right] + \frac{\bar{v}}{r^2}\left[\left(\frac{\partial\psi'}{\partial\phi}\right)^2 - \psi'\frac{\partial^2\psi'}{\partial\phi^2}\right] \end{pmatrix}, \qquad (1)$$

where *r* is the radius of the earth, *u* is the zonal wind, *v* is the meridional wind, $\overline{\boldsymbol{U}} = (\bar{u},\ \bar{v})$ is the climatological horizontal wind vector, and ψ is the geostrophic stream function at a reference latitude of ϕ_0 = 40°N. The overbars (primes) denote the basic states (perturbations), defined as the climatology (anomaly). The λ and ϕ denote the longitude and latitude, respectively. To assess the Rossby waveguide associated with the Asian jet, the meridional gradient of the climatological absolute vorticity, which is referred to as effective β (Hoskins and Ambrizzi 1993), is calculated from the climatological zonal wind. The effective β (β*) is defined as follows:

$$\beta^* \equiv \beta - \frac{1}{r^2\cos\phi}\frac{\partial}{\partial\phi}\left(\cos\phi\frac{\partial\bar{u}}{\partial\phi}\right), \qquad (2)$$

where β is the meridional gradient of the planetary vorticity. A large positive β* indicates the strong Rossby waveguide.

The RWB cases analyzed to composite in this study are the same as those extracted in TM20. They extracted 44 RWB cases over the region between [25–45°N, 130°E–180°], which is hereafter referred to as “target area”, for the period of July–August from 1958 to 2018, using a dynamical blocking index (Pelly and Hoskins 2003). The blocking index is based on the meridional distribution of potential temperature on the dynamical tropopause defined by 2 potential vorticity units (PVUs). A central date of the RWB case, when the blocking index attains its maximum, is defined as “day 0” in the lag composite analysis. A central position of the RWB case is further defined as a position where the index attains its maximum over the target area on day 0. As with TM20, the entire field was horizontally shifted before the composite analysis to sharpen the composited signatures in such a manner that the central positions of the 44 RWB cases at day 0 coincide with the reference point, which was defined as the averaged position of all the cases on day 0 (purple circle in Fig. 1).

To represent the strength of the quasi-stationary Rossby wave propagation along the Asian jet, the RWB east of Japan, and the PJ pattern, three types of indices defined by TM20 are used. The first index is the Silk Road (SR) index, defined as the 200-hPa eddy (i.e., zonal wave numbers $k \geqq 3$) kinetic energy averaged longitudinally between 60°E and 120°E and latitudinally between −5° and +5° from the 200-hPa climatological zonal wind (green shading in Fig. 1a) maxima at each longitude (black rectangle in Fig. 1a), following the procedure of Enomoto (2004). The large SR index value corresponds to the increased north–south meandering of the Asian jet, indicating enhanced propagation of the quasi-stationary Rossby waves. The second is the wave breaking (WB) index, defined as the difference in the areal averages of 350-K PV between [15–30°N, 150–170°E] (red dashed rectangle in Fig. 1a) and [30–45°N, 150–170°E] (red solid rectangle in Fig. 1a). A positive WB index value indicates RWB occurrence with reversal of the meridional gradient of the PV east of Japan, and the large index corresponds to the enhanced RWB. The third is the PJ index, defined as the difference in the areal averages of 850-hPa anomalous relative vorticity between [20–30°N, 120–150°E] (blue solid rectangle in Fig. 1a; labeled PJ1) and [30–40°N, 140–180°E] (blue dashed rectangle in Fig. 1a; labeled PJ2), which consists of the PJ1 and PJ2 indices. This study diagnoses only the PJ2 index, and the large negative PJ2 index corresponds to an enhanced lower-tropospheric anomalous anticyclone east of Japan, indicating the anomalous northwestward extension of the NPSH toward mainland Japan.

3. Lag composite analysis of persistent and non-persistent cases

This section describes results of the lag composite analysis for the cases classified by the duration of the RWB and PJ pattern. Figure 2 shows histogram of the period on which both the WB and PJ indices are positive consecutively, which is referred to as simply "duration" hereafter. The duration shown in the histogram is from 4 to 17 days in the 44 RWB cases, with the average of 8.8 day (green dashed line in Fig. 2) and the standard deviation of 3.3 day (gray shading in Fig. 2). Here the 7 longest and 7 shortest cases, with the duration greater than 11 days and shorter than 6 days, are defined as "persistent case" and "non-persistent case", respectively.

Figures 3 and 4 show the composite of the upper- and lower-tropospheric anomalous relative vorticity and 350-K PV for the persistent and non-persistent cases on day -7, -2, 0, +2, and +4, respectively. In the persistent case (Fig. 3), an anomalous anticyclone east of Japan is clearly amplified, accompanied by the strong RWB (Figs. 3a, d, g). The enhanced quasi-stationary Rossby wave propagation along the Asian jet is persistent from day -7 to day 0, contributing to the amplified RWB. The upper-level southwestward intrusion of high PV air mass toward the subtropical WNP is also clearly seen associated with the strong anticyclonic RWB (Figs. 3b, e, h). An intensified 500-hPa anomalous negative vertical p-velocity over the subtropical WNP east of the Philippines indicates enhanced convective activities, as described in section 5 using a composite of convective precipitation, immediately ahead of the southwestward intruding high PV (Figs. 3e, h, k). The enhanced convection appears to contribute to formation of the lower-tropospheric anomalous cyclonic circulation over the subtropical WNP resulting from the Matsuno-Gill-type response (Gill 1980; Figs. 3i, l). Furthermore, it is suspected that the anomalous cyclonic circulation partly contributes to an enhancement of the northeastern lower-tropospheric anomalous anticyclonic circulation due to northeastward quasi-stationary Rossby wave propagation (Red vectors in Figs. 3i, l, o; e.g., Kawamura and Ogasawara 2006), indicating a formation of the PJ pattern, consistent with the result of TM20 (see Fig. 3 in their paper). The lower-tropospheric anomalous anticyclonic circulation east of Japan associated with the dipole anomalies corresponds to the enhanced extension of the NPSH toward mainland Japan. The anomalously extended NPSH is also seen before day 0 (Figs. 3c, f), mainly because of a downward influence of the amplified anomalous anticyclone in the upper troposphere with the equivalent barotropic structure, corresponding to the formation mechanism of the Bonin high (Enomoto et al. 2003, Enomoto 2004). A vertical structure of the anomalous anticyclone shows slight northward tilt with height, accompanied by the meridional shift of its centers between the upper and lower troposphere (e.g., Figs. 3g, i), as shown in next section. Although the amplitude of the anomalies gradually declines after day 0, the structure of anomalous circulation persists until day +4 (Figs. 3j, m, l, o). An anomalous ascent at 500 hPa is also seen from Japan to the east (Figs. 3h, k), where is just below the western side of anomalous anticyclone in the upper troposphere (Figs. 3g, j), suggesting contribution of the vortex squashing effect resulting from the anomalous ascent as indicated by Wiel et al. (2015). The anomalous ascent is also presumed to be partly associated with an anomalous secondary circulation due to the zonal PV gradient between the anomalous anticyclone and an upstream trough west of Japan in the upper troposphere.

In the non-persistent case (Fig. 4), in contrast, the enhanced anomalous anticyclone east of Japan in the upper troposphere is weaker than that in the persistent case (Figs. 4a, d, g), partly because of the weaker and shorter-lived quasi-stationary Rossby wave propagation along the Asian jet before day 0. The RWB accompanied by the anomalous anticyclone east of Japan shows a rapid attenuation after day 0 (Figs. 4j, m). The upper-level southwestward intrusion of high PV air mass, the consequent anomalous ascent over the subtropical WNP east of the Philippines, and the subsequent formation of PJ pattern are also weaker and exhibit scattered structures (Figs. 4h, k, i, l), compared to the persistent case, associated with the weaker RWB. The southwest–northeast–oriented dipole anomalies in the lower troposphere, which is clearly seen in the persistent case (Figs. 3i, l), are not seen after day 0 (Figs. 4i, l), indicating rapid attenuations of the PJ pattern and the associated anomalous NPSH. The anomalous ascent in the middle troposphere along the southwestern to northern fringe of the anomalous NPSH is also not seen in the non-persistent case (Figs. 4h, k). The composite analysis for the persistent and non-persistent cases indicates that the duration is closely related to the amplified anomalous circulation in the upper troposphere and the anomalously extended NPSH, associated with the enhanced RWB and PJ pattern, respectively.

Figure 5a shows scatter diagram between maximum of WB indices and minimum of PJ2 indices, which indicates the maximum strength of RWB and extended NPSH, for the 44 RWB cases. Here, the maximum and minimum of these indices are assessed during the period from day -15 to +15. A significant relationship between the strength of RWB and the extended NPSH toward mainland Japan is seen, with a high correlation coefficient (-0.58) at a confidence level of 99%, consistent with the result of TM20. The duration of the 44 RWB cases shows that the persistent (non-persistent) case is closely related to the stronger (weaker) RWB with a correlation coefficient of +0.63 (upper panel in Fig. 5b), and to the stronger (weaker) extension of NPSH toward mainland Japan with a correlation coefficient of -0.54 (lower panel in Fig. 5b), at a confidence level of 99%. The relationship indicates that the duration is associated with the amplified anomalous anticyclone east of Japan in the troposphere. The SR indices averaged from day -6 to day -2 (Fig. 5c), when the enhanced quasi-stationary Rossby wave propagation attains its maximum before day 0, also show a relationship to the strength of RWB and extended NPSH, with correlation coefficients of +0.30 and -0.29 at a confidence level of 95%, respectively. The relationship with the SR indices (Fig. 5c) indicates that the stronger (weaker) RWB in the persistent (non-persistent) case is partly associated with the longer-lived and stronger (shorter-lived and weaker) propagation of quasi-stationary Rossby waves as shown in the composites for the persistent and non-persistent cases (Figs. 3, 4).

4. Mid-tropospheric Warm air advection related to the duration

This section shows an adiabatic contribution of anomalous thermal advection along the western to northern fringe of NPSH in the middle troposphere to persistent extension of the upper-tropospheric anomalous anticyclone east of Japan.

The duration is associated not only with the amplified anomalous anticyclone but also its vertical structure. Figure 6 shows latitude-height cross section of anomalous relative vorticity averaged between 140°E and 180° and anomalous horizontal thermal advection averaged between 130°E and 160°E on day 0 in the composite for the 44 RWB cases, the persistent and non-persistent cases. The anomalous horizontal thermal advection is expressed as follows:

$$\left[\frac{\partial T'}{\partial t}\right]_{adv} \cong -\boldsymbol{v}' \cdot \nabla\overline{T} - \overline{\boldsymbol{v}} \cdot \nabla T', \qquad (3)$$

where T is the temperature, $\boldsymbol{v}$ is the horizontal wind vector, respectively. The overbars and primes are defined as in Eq. (1). The first and second terms of the right-hand side (RHS) in Eq. (3) indicate the contributions of anomalous horizontal wind and temperature gradient to the temperature tendency, respectively. The nearly-equal relationship in Eq. (3) is because of an approximation with linear terms in the RHS of the equation, which shows cross interactions between the anomaly and the climatology, and without the self-interactions between the anomalies. Figure 6a indicates a northward tilting vertical structure of the significant anomalous anticyclone, accompanied by the upper-tropospheric amplified anticyclone at 40^{o}N associated with the RWB and the anomalous NPSH centered near 35^{o}N in the lower troposphere (green dashed line in Fig. 6). This vertical structure is consistent with the result of Kosaka and Nakamura (2006), which indicated the northward tilting vertical structure of the PJ pattern associated with the climatological zonal thermal contrast in summer. Figure 6a further shows that anomalous positive thermal advection north of 35^{o}N is seen immediately below the anomalous anticyclone in the upper troposphere, indicating anomalous warm air advection from south along the western to northern fringe of the anomalously extended NPSH. The persistent and non-persistent cases shown in Figs. 6b and 6c indicate the stronger and weaker anomalous anticyclone and warm air advection, compared to the composite (Fig. 6a), respectively.

The 500-hPa anomalous thermal advection averaged over [35–50^{o}N, 130–160^{o}E] (red rectangle labeled “A” in Fig. 1b, hereafter referred to as “region A”) on day 0 for the 44 RWB cases also shows that the stronger (weaker) anomalous warm air advection is related to the stronger (weaker) RWB with a high correlation coefficient (+0.62; upper panel in Fig. 5d), and to the stronger (weaker) extension of NPSH toward mainland Japan with a high correlation coefficient (-0.54; lower panel in Fig. 5d), at a confidence level of 99%. The anomalous warm air advection in the middle troposphere further shows significant relationship to the duration and the SR indices averaged from day -6 to day -2, with correlation coefficients of +0.34 and +0.28 at a confidence level greater than 90%, respectively (Table. 1). These results indicate that the anomalous warm air advection is closely associated with the enhanced and persistent anomalous anticyclone, and partly with the wave propagation along the Asian jet.

To examine the relationship between the duration and time variations of the northward tilting vertical structure of anomalous anticyclone, latitude-time cross sections of the anomalous relative vorticity in the upper and lower troposphere averaged between 140°E and 180° and 500-hPa anomalous thermal advection averaged between 130°E and 160°E from day -10 to +10 are shown in Fig. 7. The composite for the 44 RWB cases shown in Fig. 7a indicates slow southward shift of the significant anomalous anticyclone in the upper troposphere from north to south of 40°N, and the anomalous anticyclone is immediately above the anomalous warm air advection in the middle troposphere. The composite in the lower troposphere shown in Fig. 7b further indicates that the significant anomalous NPSH remains nearly stationary at 35°N until day +4 and then shifts southward. The anomalous warm air advection in the middle troposphere is seen north of the anomalous NPSH near

35°N. The persistent case in the upper troposphere shown in Fig. 7c indicates the enhanced and nearly stationary anomalous anticyclone at 40°N, where the anomalous warm air advection is clearly enhanced, compared to the composite (Fig. 7a). The anomalous NPSH in the persistent case shown in Fig. 7d is also amplified compared to the composite of all cases, contributing to the enhanced warm air advection in the middle troposphere to its north. The non-persistent case in the upper troposphere shown in Fig. 7e, in contrast, indicates the weaker, shorter-lived, and rapidly southward-moving anomalous anticyclone, accompanied by the much weaker anomalous warm air advection in the middle troposphere before day 0, compared to the composite (Fig. 7a). The anomalous NPSH in the non-persistent case shown in Fig. 7f is also weaker than that of the composite, and has the shorter-term duration until day +3. The northward moving anomalies in the lower troposphere are also seen south of 40°N in the non-persistent case (Fig. 7f), which is similar to the boreal summer intra-seasonal oscillation (BSISO; Kikuchi et al. 2012; Lee et al. 2013). However, there is no features of the related northward propagation of anomalous ascent in tropics as shown in the middle panels of Fig. 4, suggesting that their relevance to the BSISO is unclear.

Figure 8 further shows timeseries of vertical phase differences in the anomalous anticyclone between the lower and upper troposphere during the period from day -3 to day +3, when central latitude of the anomalous NPSH can be identified from the zonal averages of 850-hPa anomalous relative vorticity between 140°E and 180° in the non-persistent case.

Here, the vertical phase difference is defined as the difference in latitude between the minima of the anomalous relative vorticities averaged between 140°E and 180° in the latitudinal range from 20°N to 50°N at 200 hPa and 850 hPa. Positive and negative values of the vertical phase differences correspond to the northward and southward tilting vertical structure of the anomalous anticyclone. The vertical phase difference for the composite of all cases (black circles and bars in Fig. 8) indicates northward tilting vertical structure from day -3 to +3, which becomes obscure with the time evolution, corresponding to the slow southward shift of the anomalous anticyclone in the upper troposphere (Fig. 7a). In the persistent case, the vertical phase difference remains positive with the latitudinal difference of about +5°, indicating the persistence of northward tilting vertical structure even after day 0 (red circles and bars in Fig. 8). In the non-persistent case, in contrast, the vertical phase difference rapidly changes from positive to negative after day +1 (blue circles and bars in Fig. 8), indicating a transition from northward to southward tilting of the vertical structure, which is consistent with the rapid southward-moving anomalous anticyclone in the upper troposphere (Fig. 7e). The vertical phase difference of the anomalous anticyclone for the 44 RWB cases on day +2 also shows that the persistent (attenuated) northward tilting vertical structure is related to the stronger (weaker) RWB with a correlation coefficient of +0.28 (upper panel in Fig. 5e) at a confidence level of 90%, and to the stronger (weaker) extension of NPSH toward mainland Japan with a correlation coefficient of -0.40 (lower panel in Fig. 5e) at a confidence level of 99%. The vertical phase difference further shows significant relationship to the duration and the anomalous thermal advection in the middle troposphere, with correlation coefficients of +0.33 and +0.44 at a confidence level of greater than 95%, respectively (Table. 1). These results indicate that the duration is closely related to the lower- and upper-level amplified anomalous anticyclones, the associated anomalous warm air advection from south, and the persistent northward tilting vertical structure of anomalous anticyclone.

To assess the influence of the anomalous warm air advection along the fringe of the anomalously extended NPSH on the vertical motion, which can contribute to the anomalous circulation in the upper troposphere, the ***Q***-vector diagnosis (e.g., Hoskins et al. 1978, Holton 1992) is conducted for the composite circulation. The ***Q***-vector, defined in Eq. (4b) of TM20, which was incorporated into the conventional diagnostic equation for the vertical motion (i.e., the ω equation; Eq. 4a of TM20), assuming that the vertical motion is balanced with the vertical derivatives of vorticity advection and thermal advection. Convergence and divergence of the ***Q***-vectors correspond to dynamically induced ascent and descent, respectively. Figure 9a shows vertically integrated (from 850 hPa to 200 hPa) anomalous ***Q***-vectors and their divergence on day 0, which is adapted from Fig. 11 of TM20. The anomalous convergence of the ***Q***-vector is clearly seen from Japan to the east, indicating dynamically induced anomalous ascent over the region. Figure 9b shows 500-hPa anomalous thermal advection defined by Eq. (3). The anomalous warm air advection is seen immediately west to north of the anomalous anticyclonic circulation (vectors in Fig. 9b) associated with the anomalously extended NPSH. The result of thermal budget analysis indicates the relative importance of the anomalous warm air advection along the fringe of NPSH to the anomalous ascent over the region, compared to the absolute vorticity advection in the upper troposphere associated with the upstream trough west of Japan (Figs. 3g, h).

To qualitatively show a relative importance of the mid-tropospheric thermal advection and the upper-tropospheric absolute vorticity advection to the anomalous ascent from Japan to the east, a partial correlation analysis of the 44 RWB cases was performed, using adiabatic component of vertical p-velocity (ω_{adiab}) calculated from the ***Q***-vector divergence. Here, the anomalous absolute vorticity advection by a horizontal wind is defined as Eq. (5) of TM20. From the ω equation described in Eq. (4a) of TM20, the ω_{adiab} is expressed as follows:

$$\left(\nabla^2 + \frac{f_0^2}{\sigma}\frac{\partial^2}{\partial p^2}\right)\omega_{\mathrm{adiab}} \cong -\left[\frac{2}{\sigma}\nabla\cdot\boldsymbol{Q}\right], \qquad (4)$$

where f_0 is the reference Coliolis parameter at a reference latitude of ϕ_0, and ***Q*** is the ***Q***-vector, respectively. $\sigma \equiv RT_0p^{-1}d\theta_0/dp$ is the static stability, with the gas constant R and the basic-state potential temperature θ_0, derived from the area-averaged temperature T_0 north of 20°N, as with TM20. The anomalous ω_{adiab} (ω'_{adiab}) is calculated, applying a relaxation method to solve the Poisson's equation in Eq. (4), with meridional boundary conditions at 5°N and the North Pole and vertical ones at pressure levels of bottom (1000 hPa) and top (1 hPa) given by $\omega'_{\mathrm{adiab}} = 0$. Figures 10a and 10b show anomalous vertical p-velocity (ω') and ω'_{adiab} at 500 hPa on day 0, respectively. The ω'_{adiab} shown in Fig. 10b generally explains the total component of anomalous ascent from Japan to the latitudinal band of 45°N east of Japan (Fig. 10a).

Figures 11a and 11b show the relationships of areal-averaged 500-hPa anomalous thermal advection and 200-hPa anomalous absolute vorticity advection to the ω'_{adiab} over region A, without the variability associated with each other, respectively. Figure 11a shows the significant relationship between the anomalous warm air advection and anomalous ascent in the middle troposphere from Japan to the east, with a high partial correlation coefficient (−0.58) at a confidence level of 99%. The duration of the 44 RWB cases, which is represented in color in Fig. 11a, also shows its relationships to the anomalous warm air advection and ascent, with correlation coefficients of +0.35 and +0.34 at a confidence level of 95%, respectively. Although a relationship of the anomalous ascent with the anomalous absolute vorticity advection is also seen (Fig. 11b) and is consistent with the anomalous secondary circulation between the anomalous anticyclone and the upstream trough west of Japan in the upper troposphere as described in Section 3, the magnitude of the correlation coefficient is smaller than that with the anomalous thermal advection in the middle troposphere (Fig. 11a). The duration represented in color in Fig. 11b indicates that the duration has insignificant relationship (less than a confidence level of 90%) with the anomalous vorticity advection in the upper troposphere and the anomalous ascent in the middle troposphere, with low correlation coefficients of -0.11 and +0.12, respectively. The contribution rates of the thermal advection in the middle troposphere and the vorticity advection in the upper troposphere to the anomalous ascent, which were estimated from the magnitude of the standardized partial regression coefficients, are estimated as 55% and 28%, respectively. These results indicate that the anomalous warm air advection in the middle troposphere along the western to northern fringe of the anomalously extended NPSH is primarily important for the anomalous ascent by an adiabatic process and the duration. Furthermore, a multiple correlation coefficient, which is an index of how well the anomalous ascent can be explained by a linear combination of the mid-tropospheric anomalous thermal advection and the upper-tropospheric anomalous vorticity advection (e.g., Harris 1975; Mardia et al. 1979), shows a high value of +0.72 (Figs. 11a, b), indicating that the two factors can explain about half of total variations in the anomalous ascent.

5. Lower- to mid-tropospheric moisture inflow related to the duration

The anomalous southerly wind in the lower to middle troposphere along the southwestern to northern fringe of anomalously extended NPSH could be expected to cause not only the anomalous warm air advection but also the anomalous moisture inflow from the subtropical WNP (e.g., Sampe and Xie 2010), contributing to the zonally elongated anomalous ascent like the frontal zone north of the anomalous NPSH (Akiyama 1973; Kodama 1992). Hence, this section focuses on a diabatic contribution of the anomalous moisture convergence in the lower to middle troposphere to the extended anomalous anticyclone east of Japan.

Figure 12a shows the composite of vertically integrated (from 1000 hPa to 500 hPa) moisture flux (vectors) and anomalous specific humidity (shadings) on day 0. The moisture inflow is clearly seen from the subtropical WNP east of the Philippines to the sea east of Japan along the southwestern to northern fringe of the NPSH, accompanied by the anomalously moist air mass in the lower to middle troposphere. The negative ω' at 500 hPa, which is represented in purple contours in Fig. 12a, indicates zonally elongated anomalous ascent from Japan to the east, corresponding to the anomalous moisture flux convergence over the region in the lower to middle troposphere. The elongated anomalous ascent is more enhanced in the persistent case (Fig. 3), compared to the non-persistent case, as described in Section 3. Furthermore, the composite of anomalous SST averaged from day -15 to day -6, when the SST is not affected by the atmospheric circulation associate with the anomalous NPSH, shown in Fig. 12b indicates anomalous warm SST condition from the sea around Japan to its east, where the anomalously moist air and the related anomalous ascent is seen afterward (Fig. 12a). The relationship between the precedent anomalous SST and the anomalous ascent will be shown below.

To examine the relationship of the anomalous moisture convergence in the lower to middle troposphere and the anomalous warm SST to the anomalous ascent from Japan to the east, a correlation analysis with diabatic component of 500-hPa anomalous vertical p-velocity (ω'_{diab}) is performed. Here, ω'_{diab} is defined as residual difference between the ω' and ω'_{adiab}, and is expressed as follows:

$$\omega'_{\mathrm{diab}} \equiv \omega' - \omega'_{\mathrm{adiab}}. \qquad (5)$$

The ω'_{diab} at 500 hPa shown in Fig. 10c generally explains the total component of anomalous vertical motion (Fig. 10a), particularly in low latitudes. Figures 13a and 13c show the relationship of vertically integrated (from 1000 hPa to 500 hPa) moisture flux divergence on day 0 averaged over region A and anomalous SST averaged from day -15 to day -6 over [35–45°N, 130–160°E] (blue dashed rectangle labeled “B” in Fig. 1b, hereafter referred to as “region B”) to the ω'_{diab} averaged over region A on day 0 for the 44 RWB cases, respectively. Figure 13a shows a significant relationship between the moisture flux convergence in the lower to middle troposphere and the ω'_{diab} from Japan to the east, with a high correlation coefficient (+0.65) at a confidence level of 99%. The duration, which is represented in color in Fig. 13a and shown in Fig. 13b, also shows its relationship to the moisture flux convergence, with a correlation coefficient (-0.45) at a confidence level of 99%. Figures 13c and 13d, in contrast, shows an insignificant relationship (less than a confidence level of 90%) of the anomalous SST and the duration to the ω'_{diab}, with low correlation coefficients of -0.10 and +0.06, respectively. These results of the correlation analysis indicate that the moisture flux convergence from Japan to the east in the lower to middle troposphere, which is resulting from the moisture inflow along the southwestern to northern fringe of the anomalously extended NPSH rather than from surface evaporation from high SST, is primarily associated with the anomalous ascent over the region by the diabatic process.

The vertically integrated moisture flux on day 0 shown in Fig. 12a suggests that the northward moisture inflow toward east of Japan primarily originates in the subtropical WNP east of the Philippines, where the anomalous ascent is significantly seen (purple contours in Fig. 12a). Convective precipitation on day 0 shown in Fig. 12d indicates a close relationship between the anomalous ascent and the anomalous precipitation, indicating the enhanced convection over the region where the anomalous ascent is seen. It also supports the result shown in Fig. 10c indicating the essential contribution of the diabatic component (ω'_{diab}). The enhanced convection over the subtropical WNP corresponds to the dynamically induced ascent, which is resulting from the RWB east of Japan and the consequent southwestward intrusion of the upper-level high PV air mass, as indicated by TM20. The western part of the dynamically induced ascent near 20°N, 140°E particularly has a close relationship with the ω'_{diab} (Fig. 10c). Longitude-height cross section of the composite anomalous specific humidity averaged between 20°N and 25°N on day 0 shown in Fig. 12c indicates that the anomalous ascent over the subtropical WNP is associated with significantly moist conditions in the lower to middle troposphere.

To assess an impact of the lower-level moist air mass over the subtropical WNP on the anomalous ascent from Japan to the east along the fringe of the anomalously extended NPSH, a forward trajectory analysis is performed using the 6-hourly JRA-55, following to the procedure of Horinouchi (2014). In the trajectory analysis, passive tracers are horizontally advected using the second-order Heun scheme by 850-hPa horizontal winds for the composite, persistent and non-persistent cases. Here, the horizontal winds are bi-linearly interpolated in space and linearly interpolated in time from 6-hour into 15 minutes interval. Although the trajectory analysis at a pressure level can induce certain errors due to the ignored vertical transport of the tracers, the relative efficiency of the horizontal transport in a few days can be crudely compared between the three cases. The vertical displacement along the fringe of the extended NPSH, which is estimated from the vertical p-velocity at 850 hPa, actually indicates that the passive tracers for the composite remain between 850 hPa and 700 hPa in the 5-day analysis period described below (not shown). This verification result supports the validity of the trajectory analysis at a specific pressure level. The grid points over the region between [15–30°N, 130–160°E], where the composite of 500-hPa negative ω' is significant at a confidence level of 95% on initial date of day -2, is defined as the initial positions of the passive tracers, which are advected from day -2 until day +2. The trajectories initialized from day -1 and day 0 show similar results with that from day -2 (not shown). Figure 14 shows the result of trajectory analysis initialized at 00 UTC on day -2. The persistent case shown in Fig. 14a exhibits the predominant northward trajectories extending from east of the Philippines to the sea east of Japan (red lines), along the southwestern to northern fringe of the extended NPSH (contours). The non-persistent case shown in Fig. 14b, in contrast, shows the trajectories staying south of mainland Japan (blue lines) associated with the weaker extension of NPSH (contours), compared to the persistent case. The difference in the trajectories for the persistent and non-persistent cases is also clearly seen by comparing with the trajectory in the composite of 44 RWB cases (Fig. 14c). Figure 14d shows positions of the advected tracers at 18 UTC on day +2 for the persistent (red circles), non-persistent (blue crosses) cases, and the composite (green triangles). A larger number of the tracers in the persistent case is seen east of Japan, compared to the composite and the non-persistent case exhibiting the tracers from Japan to its south. The results of the trajectory analysis indicate that the enhanced anomalous ascent from Japan to the east is associated with the lower-level moist air mass over the subtropical WNP east of the Philippines, and vice versa.

Figure 13e shows the relationship between vertically integrated (from 850 hPa to 500 hPa) anomalous specific humidity averaged over [20–25^{o}N, 140–150^{o}E] (black dashed rectangle labeled “C” in Fig. 1b, hereafter referred to as “region C”) on day -2 and the ω'_{diab} over region A on day 0 for the 44 RWB cases. The scatter diagram shows the significant relationship between the anomalously moist air mass east of the Philippines in the lower to middle troposphere and the anomalous ascent from Japan to the east, with a high correlation coefficient (-0.58) at a confidence level of 99%. The duration, which is represented in color in Fig. 13e and shown in Fig. 13f, also shows its relationship to the anomalously wet conditions east of the Philippines, with a correlation coefficient of +0.26 at a confidence level of 90%, supporting the results of trajectory analysis.

6. Anomalous ascent and the duration

This section describes the influence of the anomalous ascent from Japan to the east due to the adiabatic and diabatic processes on the enhanced and persistent anomalous anticyclone in the upper troposphere. The results described in Sections 4 and 5 indicate that both the mid-tropospheric anomalous warm air advection and the lower- to mid-tropospheric moisture flux convergence from Japan to the east associated with the anomalously extended NPSH contribute to the anomalous ascent over the region, through the adiabatic and diabatic processes, respectively. A close relationship between the anomalous thermal advection and moisture inflow along the fringe of NPSH suggests a coexistence of the anomalous ascents due to the adiabatic and those due to the diabatic processes, particularly from Japan to the east in summer.

The scatter diagram of the ω'_{adiab} and ω'_{diab} at 500 hPa over region A on day 0 for the 44 RWB cases shown in Fig. 15 indicates their relationship, with a correlation coefficient of +0.40 at a confidence level of 99%. The duration, which is represented in color in Fig. 15, further shows its relationship to the ω'_{adiab} and ω'_{diab}, with the same correlation coefficients (-0.32) at a confidence level of 95%. Although the correlation coefficients can’t fully explain their relative relationship with the duration because of dependence between the ω'_{adiab} and ω'_{diab}, these results suggest the nearly equivalent associations of the anomalous ascent by the adiabatic and diabatic processes with the duration.

To show an influence of the anomalous ascent from Japan to the east on the anomalous anticyclone in the upper troposphere associated with the RWB and its relationship to the duration, a simple vorticity budget analysis is conducted. The anomalous absolute vorticity tendency associated with the vortex stretching is expressed as follows:

$$\left[\frac{\partial \xi'}{\partial \mathrm{t}}\right]_{div} \cong -\zeta' \nabla \cdot \overline{\boldsymbol{v}} - (\bar{\zeta} + f) \nabla \cdot \boldsymbol{v}', \qquad (6)$$

where ξ is the absolute vorticity, $\boldsymbol{v}$ is the horizontal wind vector, and ζ is the relative vorticity, respectively. The overbars and primes are defined as in Eq. (1). The first and second terms of RHS in Eq. (6) indicate the contributions of climatological and anomalous horizontal wind to the vorticity tendency, respectively. As with Eq. (3), Eq. (6) describes the nearly-equal relationship with an approximation by the linear terms in the RHS. The anomalous absolute vorticity tendency at 200 hPa associated with the vortex stretching shown in Fig. 9c clearly shows its negative tendency from Japan to the east, indicating the influence of the anomalous ascent on the anomalous anticyclone in the upper troposphere. To compare the vorticity tendency between the persistent and non-persistent cases, latitude-time cross sections of the anomalous relative vorticity in the upper and lower troposphere averaged between 140°E and 180° and the 200-hPa anomalous absolute vorticity tendency associated with the vortex stretching averaged between 130°E and 160°E during the period from day -10 to +10 are shown in Fig. 16. The composite in the upper troposphere shown in Fig. 16a indicates the anomalous negative vorticity tendency near 40°N, contributing to the enhanced and persistent anomalous anticyclone in the upper troposphere through the vortex squashing effect resulting from the anomalous ascent, consistent with the results of previous studies (e.g., Pfaul et al. 2015; Grams and

Archambault 2016; Wiel et al. 2015). The composite in the lower troposphere shown in Fig. 16b indicates that the negative vorticity tendency is seen immediately north of the anomalously extended NPSH, consistent with the anomalous warm air advection in the middle troposphere shown in Fig. 7b. The negative vorticity tendency near 40^{o}N is clearly seen particularly after day 0, indicating a combined effect of the anomalous warm air advection in the middle troposphere and the anomalous moisture flux convergence in the lower to middle troposphere after the occurrence of RWB and PJ pattern. The persistent case shown in Figs. 16c and 16d exhibits the enhanced anomalous negative vorticity tendency at 40^{o}N particularly after day 0, compared to the composite (Figs. 16a, b), indicating its stronger influence on the enhancement and persistence of the anomalous anticyclone in the upper troposphere. The non-persistent case shown in Figs. 16e and 16f, in contrast, indicates the quite weaker anomalous negative vorticity tendency after day 0, compared to the composite. The non-persistent case further shows anomalous positive vorticity tendency at 40^{o}N from day -4 to day 0, contributing to the weak and transient anomalous anticyclone in the upper troposphere (Fig. 16e). Figure 5f shows the relationship of the maximum of WB indices and the minimum of PJ2 indices to the 200-hPa anomalous absolute vorticity tendency associated with the vortex stretching averaged over region B on day 0 for the 44 RWB cases. It also shows that the anomalous vortex squashing in the upper troposphere resulting from the anomalous ascent is closely associated with the strong RWB east of Japan (upper panel in Fig. 5f) and the extension of

NPSH toward mainland Japan (lower panel in Fig. 5f), with high correlation coefficients of -0.45 and +0.50 at a confidence level of 99%, respectively. The anomalous vortex squashing further shows significant relationship to the duration, the anomalous thermal advection in the middle troposphere, and the persistent vertical phase difference of the anomalous anticyclone, with correlation coefficients of -0.28, -0.53, and -0.45 at a confidence level of greater than 90%, respectively (Table. 1).

These results described in this section indicate that the anomalous ascent from Japan to the east, which is resulting from the mid-tropospheric anomalous warm air advection and the lower- to mid-tropospheric anomalous moisture inflow along the fringe of the anomalously extended NPSH, contributes to the enhancement and persistence of anomalous anticyclone in the upper troposphere and hence the associated duration of RWB.

7. Conclusion and discussion

To reveal the maintenance mechanism for the RWB accompanied by the anomalous anticyclone east of Japan in the upper troposphere and the PJ pattern, which are triggered by the mechanism indicated in TM20, we analyzed the past 44 RWB cases east of Japan extracted in TM20. Here, the trigger mechanism described in TM20 is summarized schematically in Fig. 17a for the comprehensive understanding of the maintenance mechanism shown in this study. The persistent and non-persistent cases are defined as the cases which the RWB and PJ pattern were simultaneously seen during the period longer than 11 days and shorter than 6 days, respectively, using the WB and PJ indices. Compared to the non-persistent case, the persistent case indicated the stronger and longer-lived quasi-stationary Rossby wave propagation along the Asian jet, corresponding to the stronger RWB and the consequent formation of the more enhanced PJ pattern through the high PV intrusion toward the subtropical WNP. The persistent case further indicated the persistent northward tilting vertical structure of the anomalous anticyclone east of Japan, accompanied by the enhanced anomalous warm air advection in the lower to middle troposphere immediately north of the anomalously extended NPSH. The ***Q***-vector diagnosis and the partial correlation analysis indicated that the anomalous warm air advection in the middle troposphere was closely associated with the dynamically induced anomalous ascent from Japan to the east by an adiabatic process, and anomalous positive absolute vorticity advection in the upper troposphere plays a smaller role. The results of forward trajectory analysis and correlation analysis indicate that the enhanced moisture flux convergence from Japan to the east, which was associated with the moisture inflow from the subtropical WNP along the southwestern to northern fringe of the anomalously extended NPSH, also contributes to the anomalous ascent over the region by a diabatic process. The zonally elongated anomalous ascent from Japan to the east, which is similar to the frontal zone north of the NPSH, has a same feature indicated by Sampe and Xie (2010), which showed an essential role of the warm advection in the middle troposphere on a formation of the Baiu frontal zone. The warm and moist air inflow and the consequent front-like zone of ascent from Japan to the east are consistent with the increased tendency of line-shaped rainbands over northern Japan during boreal summer in La Niña years partly because of the anomalously northward shifted Baiu front (Yamada et al. 2012). This feature further corresponds to the favorable condition of the RWB cases east of Japan in La Niña-like anomalous SST over the equatorial central to eastern Pacific, as indicated by TM20. A simple correlation analysis suggested nearly equivalent associations of the adiabatic and diabatic factors of anomalous ascent with the duration. The persistent case further indicated strong negative vorticity tendency resulting from the anomalous ascent from Japan to the east, contributing to the enhancement and persistence of the anomalous anticyclone in the upper troposphere associated with the RWB. The results of this study propose a conceptual model for the maintenance mechanism of the RWB east of Japan and the PJ pattern, which is summarized schematically in Fig. 17b.

The processes that the RWB, which is triggered by the mechanism of TM20 (Fig. 17a) and is sustained by the anomalous ascent north of the anomalous NPSH, can recursively affect the enhancement and persistence of PJ pattern through the high PV intrusion toward the subtropical WNP. If this process exists, it will be one of the interesting mechanisms to be further examined in terms of the so-called positive feedback mechanism between the RWB and PJ pattern. The anomalous ascent by the diabatic process was closely associated with the moisture inflow from the subtropical WNP, where the dynamically induced ascent and the consequential moist conditions resulting from the RWB were seen. The maintenance mechanism shown in this study indicates an essential role of the interaction between extratropical and tropical variabilities and that between the upper and lower tropospheric anomalous circulation on the duration of the RWB and the PJ pattern, and hence on the persistent abnormal weather conditions over the region in boreal summer.

Acknowledgments

The authors are very grateful to two anonymous reviewers for their constructive and helpful comments. The Generic Mapping Tools (GMT) were used to create the graphics. This study was partly supported by the JSPS KAKENHI Grant (18H01280, 18K03734).

References

Abatzoglou, J. T., and G. Magnusdottir, 2006: Planetary wave breaking and nonlinear reflection: Seasonal cycle and interannual variability. *J. Climate*, **19**, 6139–6152.

Akiyama, T., 1973: The large-scale aspects of the characteristic features of the Baiu front. *Pap. Meteor. Geophys.*, **24** (2), 157–188.

Duchon, C. E, 1979: Lanczos filtering in one and two dimensions. *J. Appl. Meteor.*, **18**, 1016–1022.

Enomoto, T., B. J. Hoskins, and Y. Matsuda, 2003: The formation mechanism of the Bonin high in August. *Quart. J. Roy. Meteor. Soc.*, **129**, 157–178.

Enomoto, T., 2004: Interannual variability of the Bonin high associated with the propagation of Rossby waves along the Asian jet. *J. Meteor. Soc. Japan*, **82**, 1019–1034.

Gill, A. E., 1980: Some simple solutions for heat-induced tropical circulation. *Quart. J. Roy. Meteor. Soc.*, **106**, 447-462.

Grams, C. M., and H. M. Archambault, 2016: The key role of diabatic outflow in amplifying the midlatitude flow: A representative case study of weather systems surrounding western North Pacific extratropical transition. *Mon. Wea. Rev.*, **144**, 3847–3869.

Harris, R. J., 1975: *A primer of multivariate statistics*. Academic Press.

Hitchman, M. H., and A. S. Huesmann, 2007: A seasonal climatology of Rossby wave breaking in the 320-2000-K layer. *J. Atmos. Sci.*, **64**, 1922–1940.

Holton, J. R., 1992: *An Introduction to Dynamic Meteorology, 3rd ed*. Academic Press, 507pp.

Homeyer, C. R., and K. P. Bowman, 2013: Rossby wave breaking and transport between the tropics and extratropics above the subtropical jet. *J. Atmos. Sci.*, **70**, 607–626.

Horinouchi, T., 2014: Influence of upper tropospheric disturbances on the synoptic variability of precipitation and moisture transport over summertime East Asia and the northern Pacific. *J. Meteor. Soc. Japan*, **92**, 519–541.

Hoskins, B. J., and T. Ambrizzi, 1993: Rossby wave propagation on a realistic longitudinally varying flow. *J. Atmos. Sci.*, **50**, 1661–1671.

Hoskins, B. J., I. Draghici, and H. C. Davies, 1978: A new look at the ω-equation. *Quart. J. R. Met. Soc.*, **104**, 31–38.

Ishii, M., A. Shouji, S. Sugimoto, and T. Matsumoto, 2005: Objective analyses of sea-surface temperature and marine meteorological variables for the 20th century using ICOADS and the Kobe collection. *Int. J. Climatol.*, **25**, 865–879.

Kawamura, R., M. Sugi, T. Kayahara, and N. Sato, 1998: Recent extraordinary cool and hot summers in East Asia simulated by an ensemble climate experiment. *J. Meteor. Soc. Japan*, **76**, 597–617.

Kawamura, R., T. Matsuura, and S. Iizuka, 2001: Interannual atmosphere-ocean variations in the tropical western North Pacific relevant to the Asian summer monsoon-ENSO coupling. *J. Meteor. Soc. Japan*, **79**, 883–898.

Kawamura, R., and T. Ogasawara, 2006: On the role of typhoons in generating PJ teleconnection patterns over the western North Pacific in late summer. *SOLA*, **2**, 37–40.

Kikuchi, K., B. Wang, and Y. Kajikawa, 2012: Bimodal representation of the tropical intraseasonal oscillation. *Climate Dyn.*, **38**, 1989-2000, doi:10.1007/s00382-011-1159-1.

Kobayashi, S., Y. Ota, Y. Harada, A. Ebita, M. Moriya, H. Onoda, K. Onogi, H. Kamahori, C. Kobayashi, H. Endo, K. Miyaoka, and K. Takahashi, 2015: The JRA-55 reanalysis: General specifications and basic characteristics. *J. Meteor. Soc. Japan*, **93**, 5−48.

Kodama, Y.-M., 1992: Large-scale common features of subtropical precipitation zones (the Baiu frontal zone, the SPCZ, and the SACZ). Part I: Characteristics of subtropical frontal zones. *J. Meteor. Soc. Japan*, **70**, 813–836.

Kosaka, Y., and H. Nakamura, 2006: Structure and dynamics of the summertime Pacific-Japan teleconnection pattern. *Quart. J. R. Met. Soc.*, **132**, 2009–2030.

Lee, J. T., B. Wang, M. C. Wheeler, X. Fu, D. E. Waliser, and I.-S. Kang, 2013: Real-time multivariate indices for the boreal summer intraseasonal oscillation over the Asian summer monsoon region. *Climate Dyn.*, **40**, 493-509, doi:10.1007/s00382-012-1544-4.

Liu, B., C. Zhu, J. Su, S. Ma, and K. Xu, 2019: Record-breaking northward shift of the western North Pacific subtropical high in July 2018. *J. Meteor. Soc. Japan*, **97**, 913–925.

Lu, R., and B. W. Dong, 2001: Westward extension of North Pacific subtropical high in summer. *J. Meteor. Soc. Japan*, **79**, 1229–1241.

Lu, R., 2002: Indices of the summertime western North Pacific subtropical high. *Adv. Atmos, Sci.*, **19**, 1004–1028.

Lu, R.-Y., J.-H. Oh, and B.-J. Kim, 2002: A teleconnection pattern in upper-level meridional wind over the North African and Eurasian continent in summer, *Tellus*, **54**, 44–55. doi:10.3402/tellusa.v54i1.12122.

Mardia, K. V., J. T. Kent, and J. M. Bibby, 1979: *Multivariate analysis*. Academic Press.

Ninomiya, K., and C. Kobayashi, 1999: Precipitation and moisture balance of the Asian summer monsoon in 1991. Part II: Moisture transport and moisture balance. *J. Meteor. Soc. Japan*, **77**, 77–99.

Nitta, T., 1987: Convective activities in the tropical western Pacific and their impact on the

Northern Hemisphere summer circulation. *J. Meteor. Soc. Japan*, **65**, 373–390.

Pelly, J. L., and B. J. Hoskins, 2003: A new perspective on blocking. *J. Atmos. Sci.*, **60**, 743–755.

Pfahl, S., C. Schwierz, M. Croci-Maspoli, C. M. Grams, and H. Wernli, 2015: Importance of latent heat release in ascending air streams for atmospheric blocking. *Nat. Geosci.*, **8**, 610–614, doi:10.1038/ngeo2487.

Postel, G. A., and M. H. Hitchman, 1999: A climatology of Rossby wave breaking along the subtropical tropopause. *J. Atmos. Sci.*, **56**, 359–373.

Postel, G. A., and M. H. Hitchman, 2001: Observational diagnosis of a Rossby wave breaking event along the subtropical tropopause. *Mon. Wea. Rev.*, **129**, 2555–2569.

Rodwell, M. J., and B. J. Hoskins, 2001: Subtropical anticyclones and summer monsoons. *J. Climate*, **14**, 3192–3211.

Sampe, T., and S.-P. Xie, 2010: Large-scale dynamics of the Meiyu-Baiu rainband: Environmental forcing by the westerly jet. *J. Climate*, **23**, 113–134.

Shimpo, A., K. Takemura, S. Wakamatsu, H. Togawa, Y. Mochizuki, M. Takekawa, S. Tanaka, K. Yamashita, S. Maeda, R. Kurora, H. Murai, N. Kitabatake, H. Tsuguti, H. Mukougawa, T. Iwasaki, R. Kawamura, M. Kimoto, I. Takayabu, Y. N. Takayabu, Y. Tanimoto, T. Hirooka, Y. Masumoto, M. Watanabe, K. Tsuboki, and H. Nakamura, 2019: Primary factors behind the Heavy Rain Event of July 2018 and the subsequent heat wave in Japan. *SOLA*, **15A**, 13–18.

Takaya, K., and H. Nakamura, 2001: A formulation of a phase-independent wave-activity flux for stationary and migratory quasigeostrophic eddies on a zonally varying basic flow. *J. Atmos. Sci.*, **58**, 608–627.

Takemura, K., and H. Mukougawa, 2020: Dynamical relationship between quasi-stationary Rossby wave propagation along the Asian jet and Pacific-Japan pattern in boreal summer. *J. Meteor. Soc. Japan*, **98**, https://doi.org/10.2151/jmsj.2020-010.

Wakabayashi, S., and R. Kawamura, 2004: Extraction of major teleconnection patterns possibly associated with anomalous summer climate in Japan. *J. Meteor. Soc. Japan*, **82**, 1577–1588.

Wiel, K. V., A. J. Matthews, D. P. Stevens, and M. M. Joshi, 2015: A dynamical framework for the origin of the diagonal South Pacific and South Atlantic convergence zones. *Quart. J. Roy. Meteor. Soc.*, **141**, 1997–2010.

Xu, P., L. Wang, W. Chen, J. Feng, and Y. Liu, 2019: Structural changes in the Pacific-Japan pattern in the late 1990s. *J. Climate*, **32**, 607–621.

Yamada, T. J., J. Sasaki, N. Matsuoka, 2012: Climatology of line-shaped rainbands over northern Japan in boreal summer between 1990 and 2010. *Atmospheric Science Letters*, **13**, 133–138.

List of Tables

Table. 1. Summary of correlation coefficients between the duration (unit: day), SR index (unit: $m^2\ s^{-2}$) averaged from day -6 to day -2, 500-hPa anomalous horizontal thermal advection (unit: 10^{-6} K s^{-1}) averaged over region A (Fig. 1b) on day 0, vertical phase differences (unit: degree) in the anomalous anticyclone over 140°E–180° between 850 hPa and 200 hPa on day +2, and 200-hPa anomalous absolute vorticity tendency associated with the vortex stretching (unit: $10^{-11}\ s^{-2}$) averaged over region B on day 0. Bold face indicates the correlation coefficient exceeding a confidence level of 90%.

	SR index	500-hPa anomalous thermal advection	Vertical phase difference	200-hPa anomalous vorticity tendency
Duration	+0.19	**+0.34***	**+0.33***	**-0.28**
SR index		**+0.28**	+0.23	-0.16
500-hPa anomalous thermal advection			**+0.44****	**-0.53****
Vertical phase difference				**-0.45****

* Confidence level exceeding 95%.

** Confidence level exceeding 99%.

List of Figures

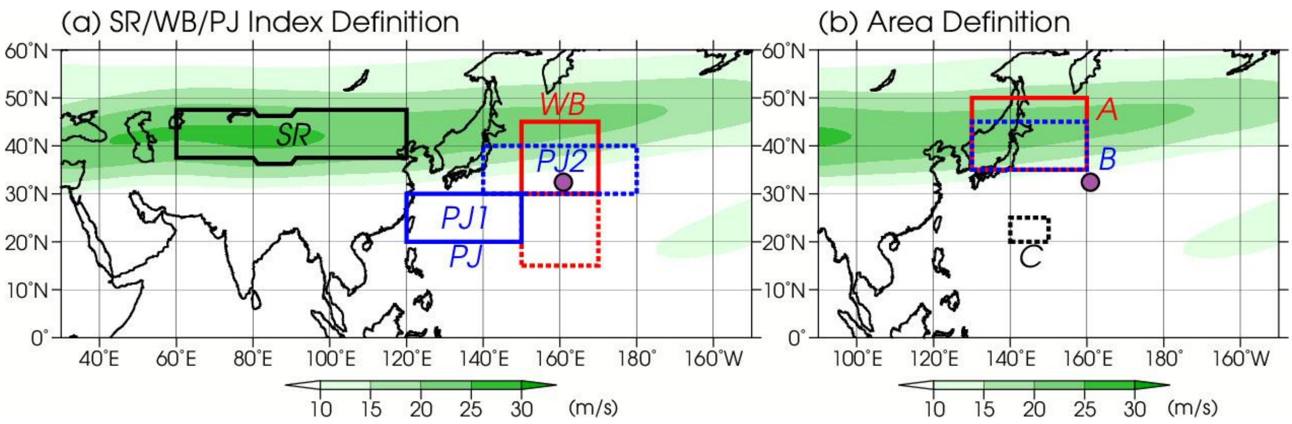

Fig. 1. (a) Defined region for SR, WB, and PJ indices, and (b) the region labeled A, B, and C used to calculate areal averages. The southern and northern parts of the region to calculate the PJ index are labeled PJ1 and PJ2, respectively. Green shading indicates the 200-hPa climatological zonal wind (unit: m s^{-1}). Purple circles in (a) and (b) indicate the averaged position of the 44 RWB cases. See text for the definition of the SR, WB and PJ indices. (a) is based on Takemura and Mukougawa (2020).

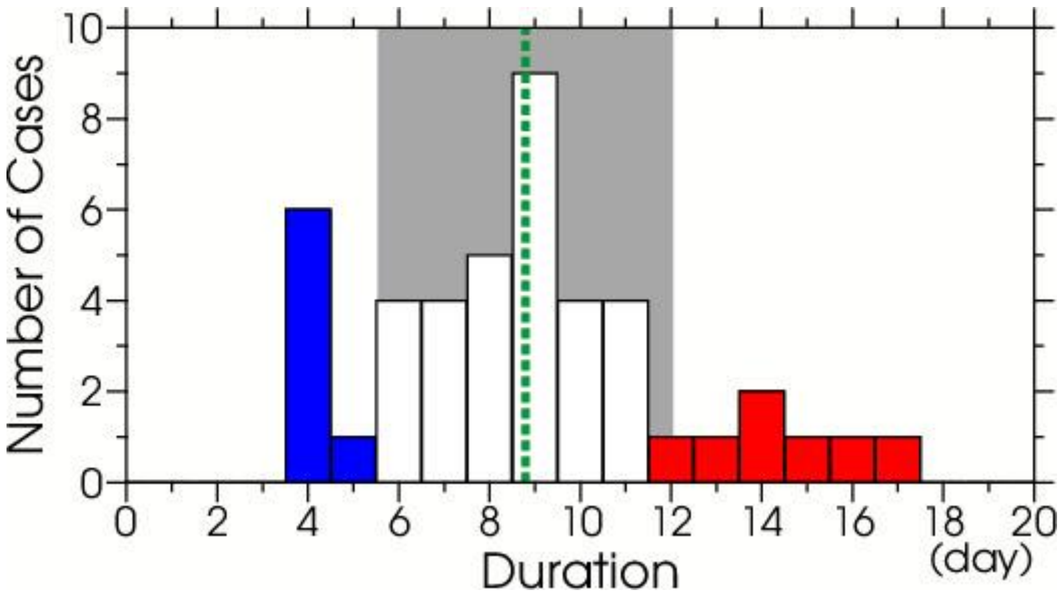

Fig. 2. Histogram of duration (unit: day) for RWB and PJ pattern in the 44 RWB cases. Red and blue bars indicate 7 persistent cases and 7 non-persistent cases with the duration greater than 11 days and shorter than 6 days, respectively. Green dashed line and gray shading indicate average and standard deviation of the duration for the 44 RWB cases, respectively.

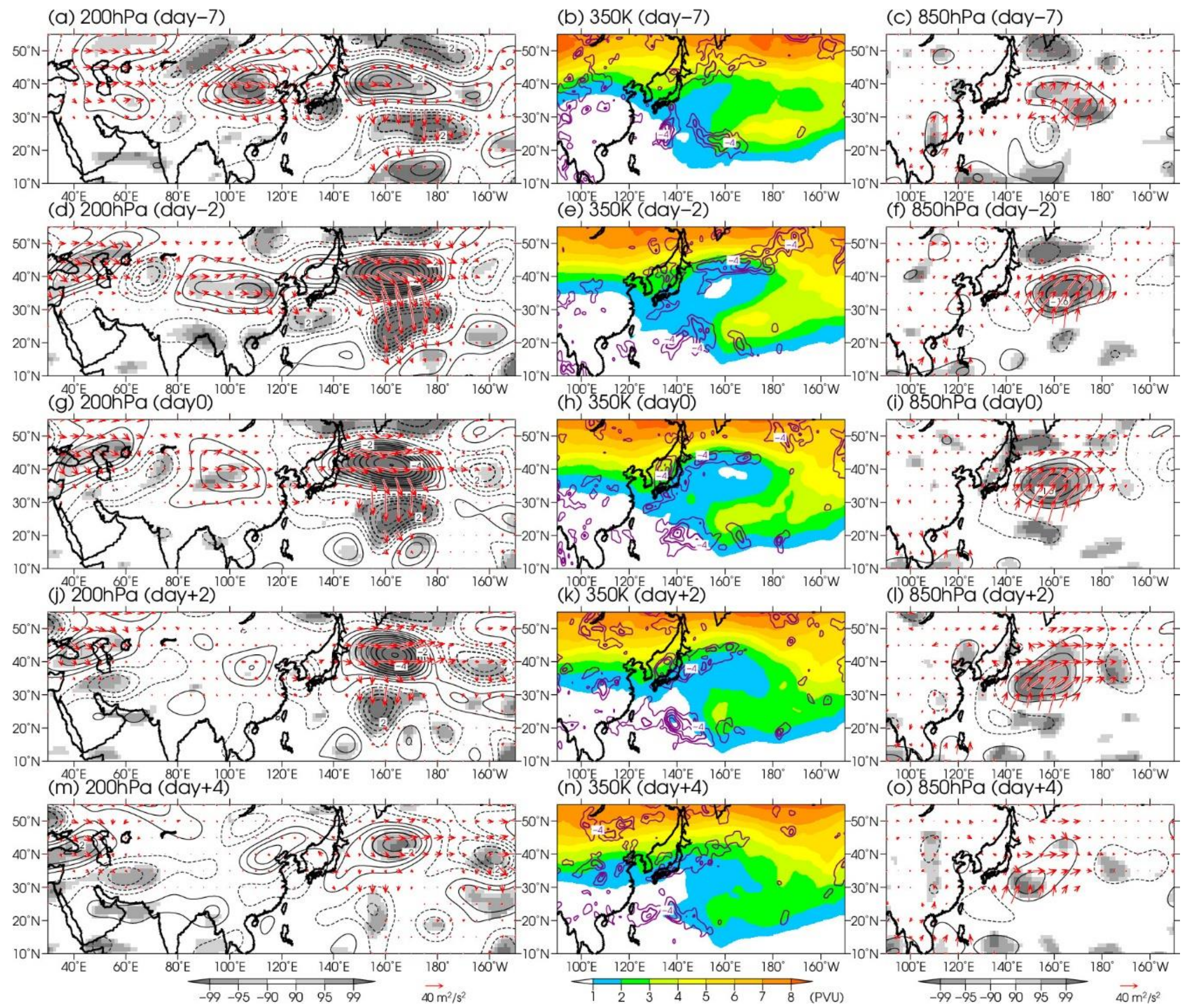

Fig. 3. Composite of 5-day averaged (left) 200-hPa anomalous relative vorticity (contour interval: 0.5×10^{-5} s^{-1}), (middle) 350-K potential vorticity (shading; unit: PVU), 500-hPa anomalous negative vertical p-velocity (purple contour; interval: 2×10^{-2} Pa s^{-1}), and (right) 850-hPa anomalous relative vorticity (contour interval: 0.4×10^{-5} s^{-1}) for the persistent case. Solid and dashed contours on the left and right panels denote negative and positive vorticity anomalies, respectively. Red vectors indicate the WAF (unit: m^2 s^{-2}). Gray shading on the left and right panels indicates significance levels of the anomalous relative vorticity. (a, b, c) day −7, (d, e, f) day −2, (g, h, i) day 0, (j, k, l) day +2, and (m, n, o) day +4.

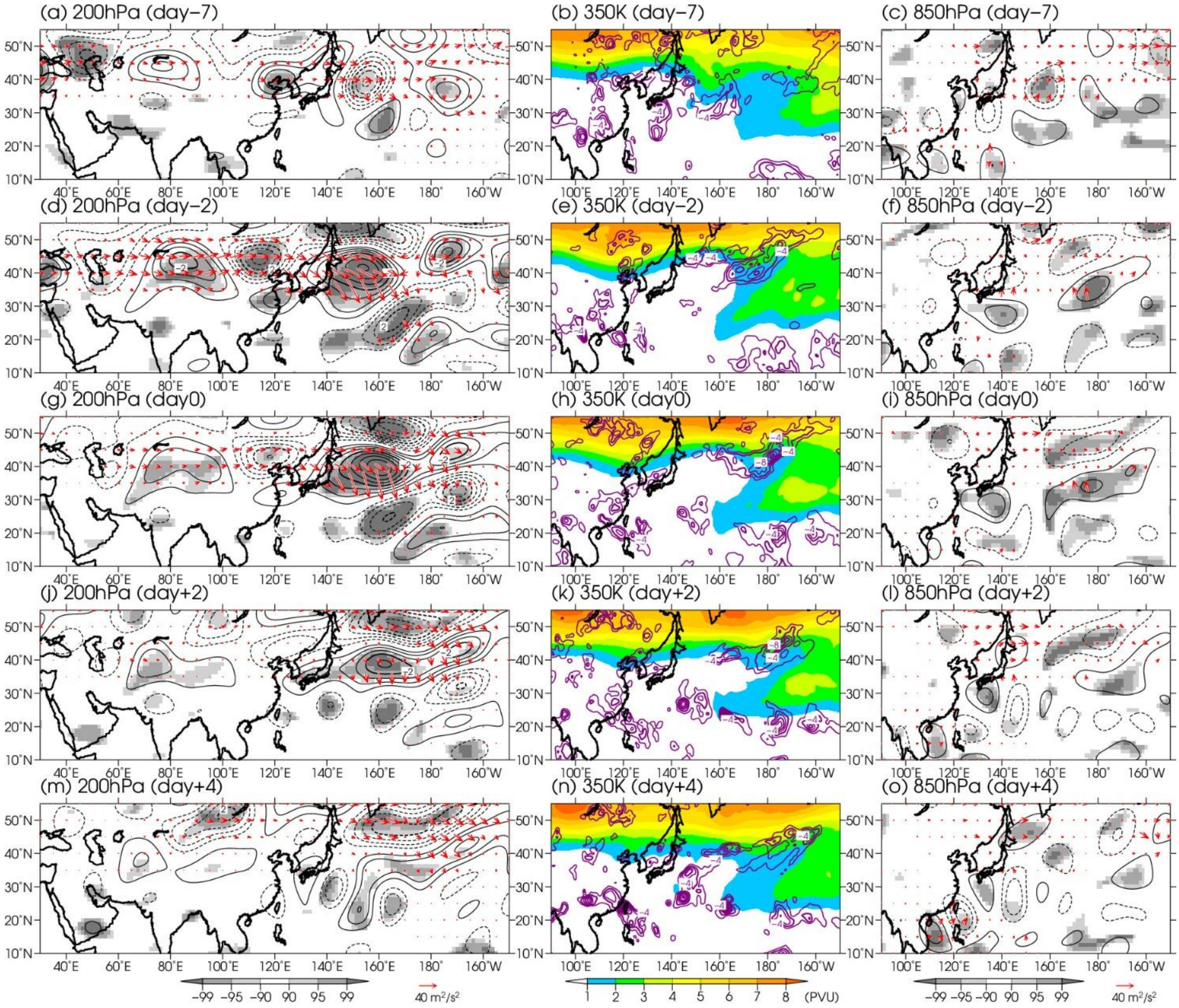

Fig. 4. Same as Fig. 3, but for the non-persistent case.

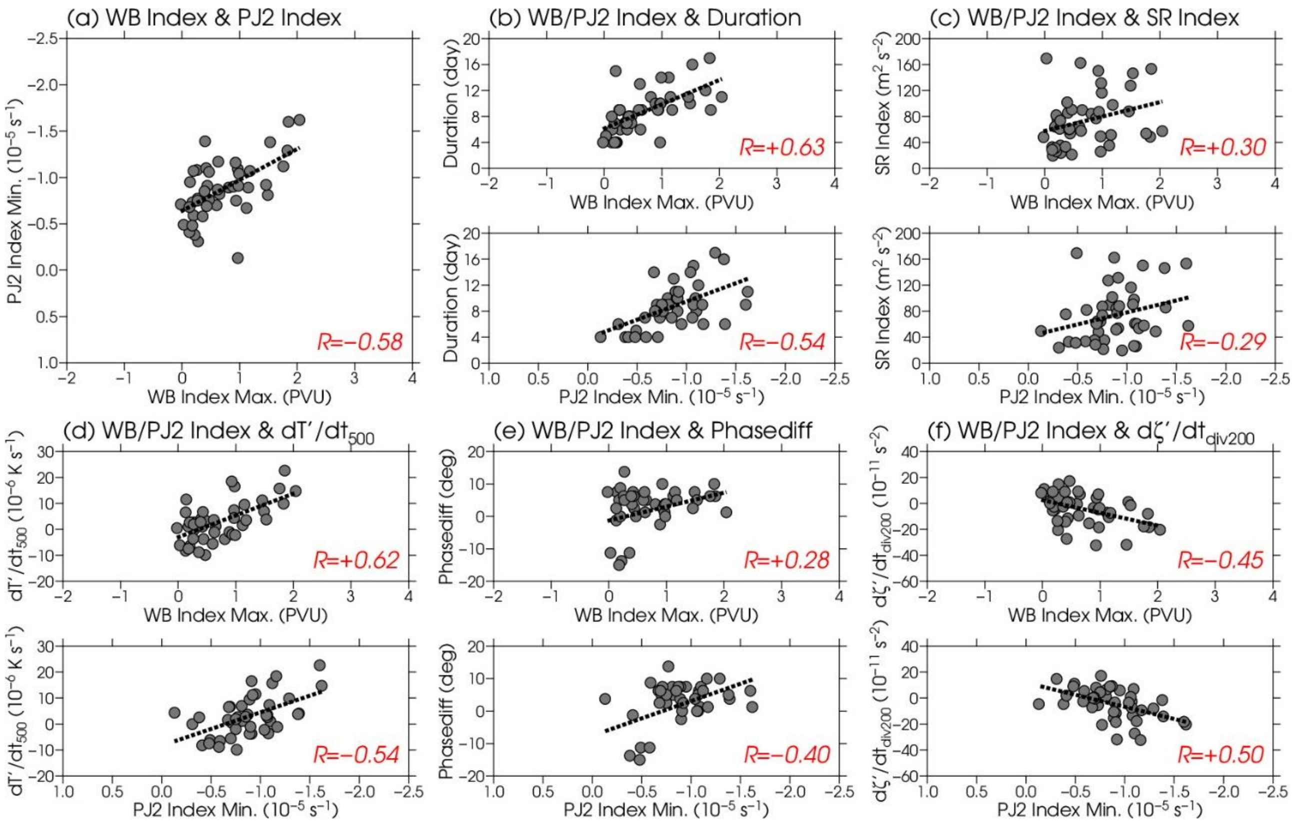

Fig. 5. Scatter diagram of 5-day averaged (a) maximum of WB index (X-axis; unit: PVU) and minimum of PJ2 index (Y-axis; unit: 10^{-5} s^{-1}), and their relationships to (b) the duration (unit: day), (c) SR index (unit: m^2 s^{-2}) averaged from day -6 to day -2, (d) 500-hPa anomalous horizontal thermal advection (unit: 10^{-6} K s^{-1}) averaged over region A (Fig. 1b) on day 0, (e) vertical phase differences (unit: degree) in the anomalous anticyclone over 140^{o}E–180^{o} between 850 hPa and 200 hPa on day +2, and (f) 200-hPa anomalous absolute vorticity tendency associated with the vortex stretching (unit: 10^{-11} s^{-2}) averaged over region B (Fig. 1b) on day 0 for the 44 RWB cases. The maximum of WB index and the minimum of PJ2 index are assessed during the period from day -15 to +15. In (b)–(f), X-axes on the upper and lower panels show the maximum of WB index and the minimum of PJ2 index, respectively. Dashed lines denote regression lines of Y-

on X-components, with a confidence level of the correlation coefficients between the two components greater than 90%. *R* shown at the lower right of each panel is the corresponding correlation coefficient between X- and Y-components.

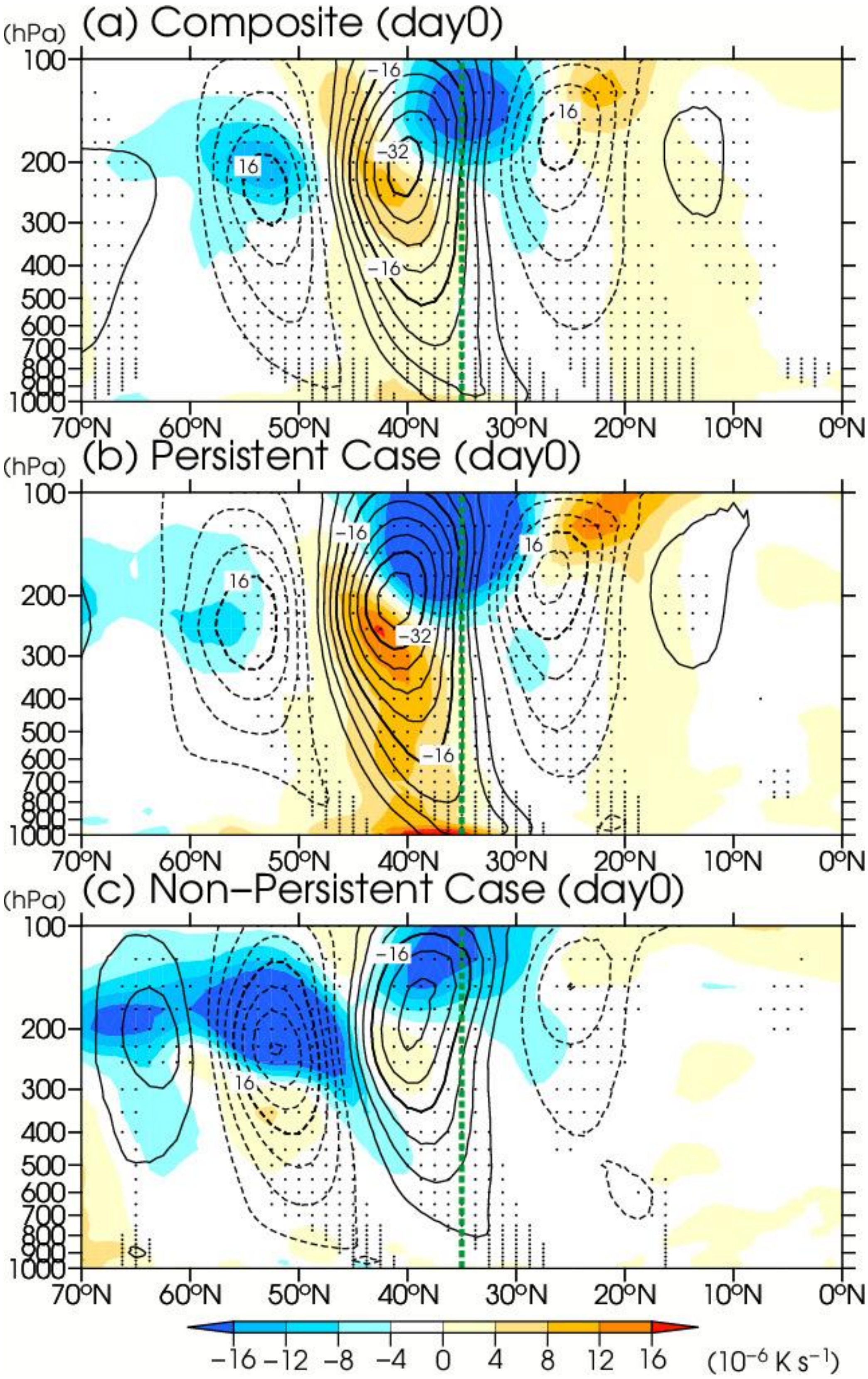

Fig. 6. Latitude-height cross sections of 5-day averaged anomalous relative vorticity (contour interval: 4 × 10^{-6} s^{-1}) averaged between 140°E and 180° and anomalous

horizontal thermal advection (shading; unit: 10^{-6} K s^{-1}) averaged between 130^{o}E and 160^{o}E in (a) the composite for the 44 RWB cases, (b) the persistent case, and (c) the non-persistent case. Solid and dashed contours denote negative and positive vorticity anomalies, respectively. Dots indicate statistical significance at a 95% confidence level of the composite anomalous relative vorticity. Green dashed lines denote a latitude line of 35^{o}N, where is near the center of anomalous anticyclone at 850 hPa.

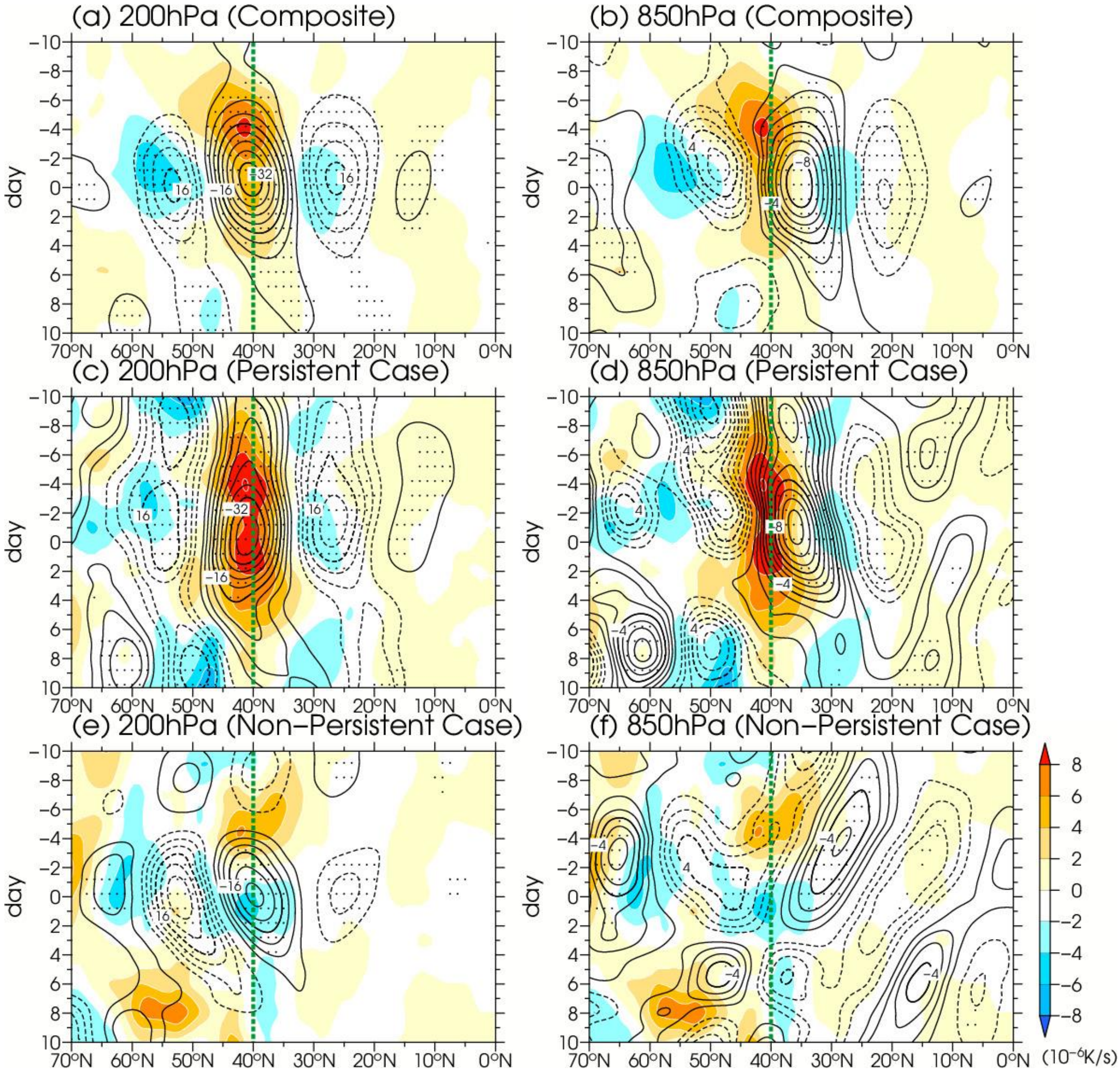

Fig. 7. Latitude-time cross section of 5-day averaged anomalous relative vorticity (contour; unit: 10^{-6} s^{-1}) averaged between 140°E and 180° and 500-hPa anomalous horizontal thermal advection (shading; unit: 10^{-6} K s^{-1}) averaged between 130°E and 160°E from day -10 to day +10 in (a, b) the composite for the 44 RWB cases, (c, d) the persistent case, and (e, f) the non-persistent case. Left and right panel shows the anomalous relative vorticities at 200 hPa and 850 hPa with the contour intervals of 4×10^{-6} s^{-1} and 1×10^{-6} s^{-1}, respectively. Solid and dashed contours denote negative and positive vorticity

anomalies, respectively. Dots indicate statistical significance at a 95% confidence level of the composite anomalous relative vorticity. Green dashed lines denote a latitude line of 40°N, where is a central position of the anomalous anticyclone in the upper troposphere on day 0.

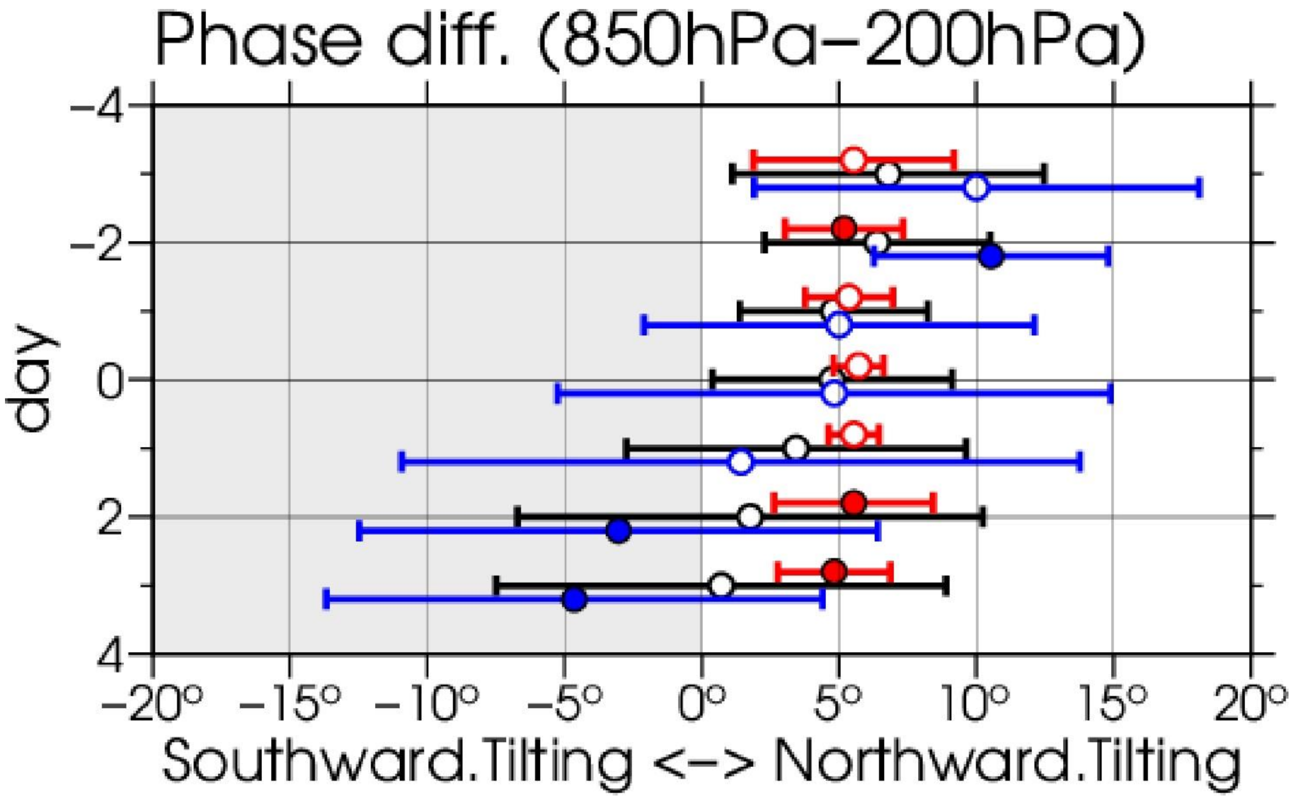

Fig. 8. Timeseries of vertical phase differences (VPDs; unit: degree) in the anomalous anticyclone over 140^{o}E–180^{o} between 850 hPa and 200 hPa from day -3 to day +3. See text for the detailed definition of the VPD. Black-, red-, and blue-colored circles and bars denote the VPDs and its standard deviations for the composite of the 44 RWB cases, the persistent case, and the non-persistent case, respectively. The positive and negative VPDs indicate the northward and southward tilting vertical structure of the anomalous anticyclone, respectively. Red- and blue-colored closed circles indicate that the difference in the VPDs between the persistent and non-persistent cases is significant at a confidence level of 95%.

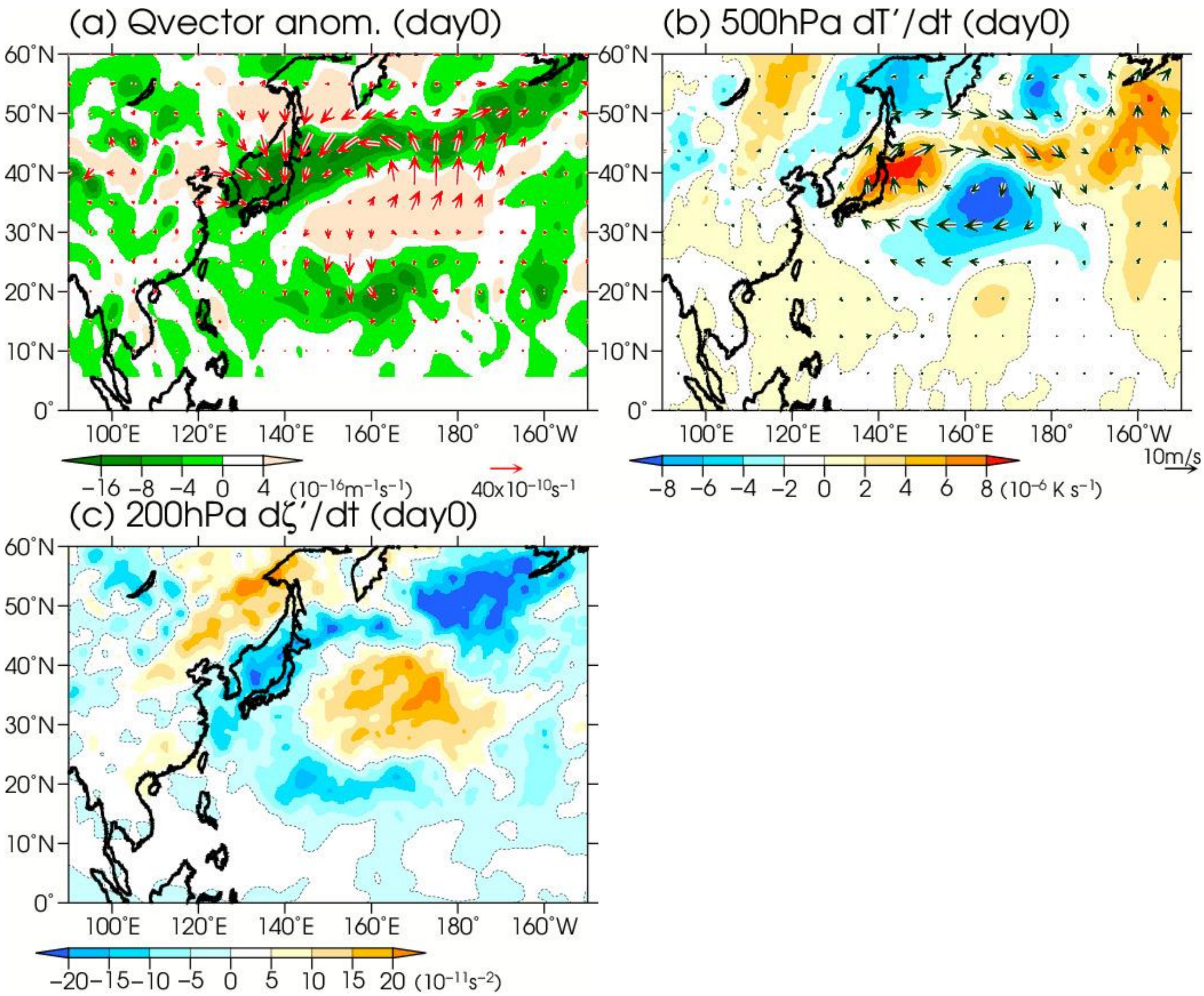

Fig. 9. Composite of (a) vertically integrated anomalous ***Q***-vectors (vectors; unit: s^{-1}) and their divergence (shading; unit: m^{-1} s^{-1}) over a region north of 5°N derived from 5-day averages, (b) 5-day averaged 500-hPa anomalous horizontal thermal advection (shading; unit: 10^{-6} K s^{-1}) and anomalous horizontal wind (vectors; unit: m s^{-1}), and (c) 5-day averaged 200-hPa anomalous absolute vorticity tendency associated with the vortex stretching (unit: 10^{-11} s^{-2}) on day 0. Green shading in (a) indicates the convergence of the ***Q***-vector. The vertical integration in (a) is taken from 850 hPa to 200 hPa. (a) is adapted from Takemura and Mukougawa (2020).

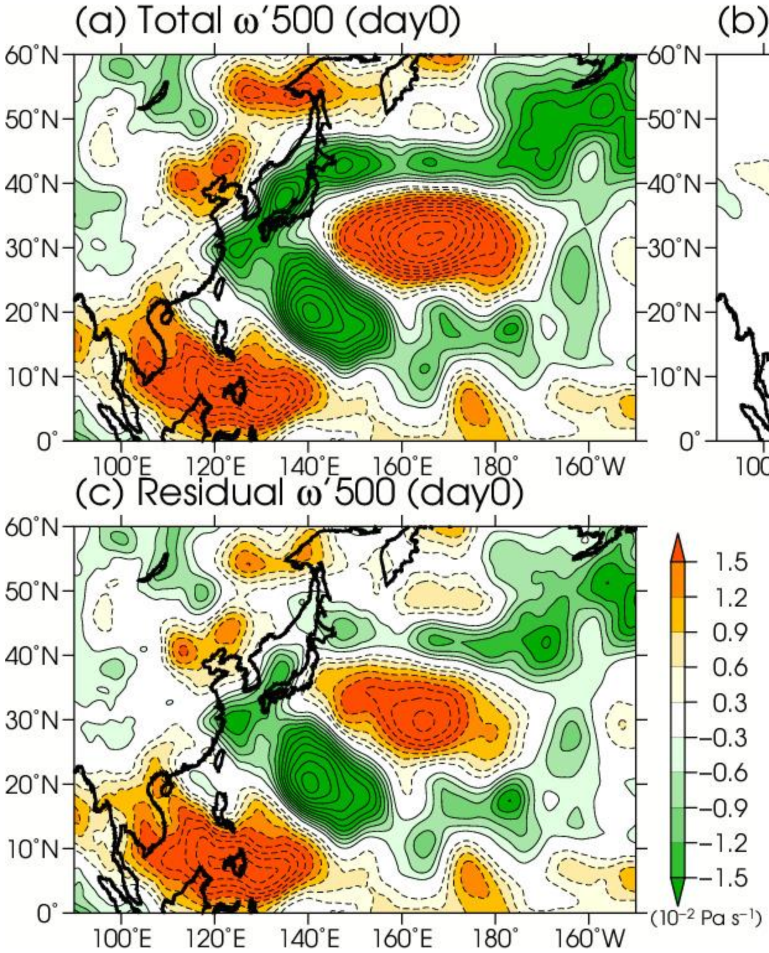

Fig. 10. Composite of 5-day averaged 500-hPa anomalous (a) total, (b) adiabatic (ω'_{adiab}) and (c) the residual (i.e., diabatic; ω'_{diab}) components of vertical p-velocity (unit: 10^{-2} Pa s^{-1}) on day 0.

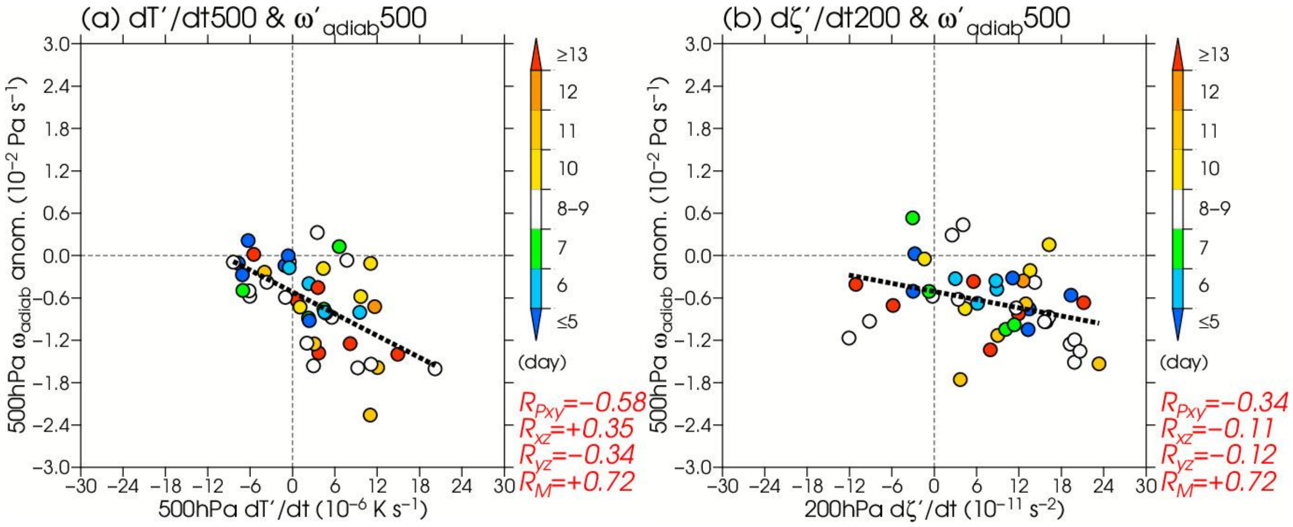

Fig. 11. Scatter diagram of 5-day averaged (a) 500-hPa anomalous thermal advection (X-axis; RHS in Eq. 3; unit: 10^{-6} K s^{-1}), (b) 200-hPa anomalous vorticity advection (X-axis; RHS in Eq. 5 of TM20; unit: 10^{-11} s^{-2}) and adiabatic component of 500-hPa anomalous vertical p-velocity (ω'_{adiab}; Y-axis; unit: 10^{-2} Pa s^{-1}) averaged over region A (Fig. 1b) on day 0 for the 44 RWB cases. In (a) and (b), the variability explained by the 200-hPa anomalous vorticity advection and the 500-hPa anomalous thermal advection is removed, respectively, using the partial regression. Dashed lines denote regression lines of Y- on X-components, with a confidence level of the correlation coefficients between the two components greater than 90%. Colors represent the duration (unit: day), which is referred to as Z-component. The corresponding partial correlation coefficient between X- and Y-components (R_{Pxy}), correlation coefficients between X- and Z-components (R_{xz}), Y- and Z-components (R_{yz}), and multiple correlation coefficient (R_M) are shown at the lower right of each panel. Sign of R_{yz} in text is reversed to represent the relationship to the anomalous ascent (i.e., negative ω'_{adiab}).

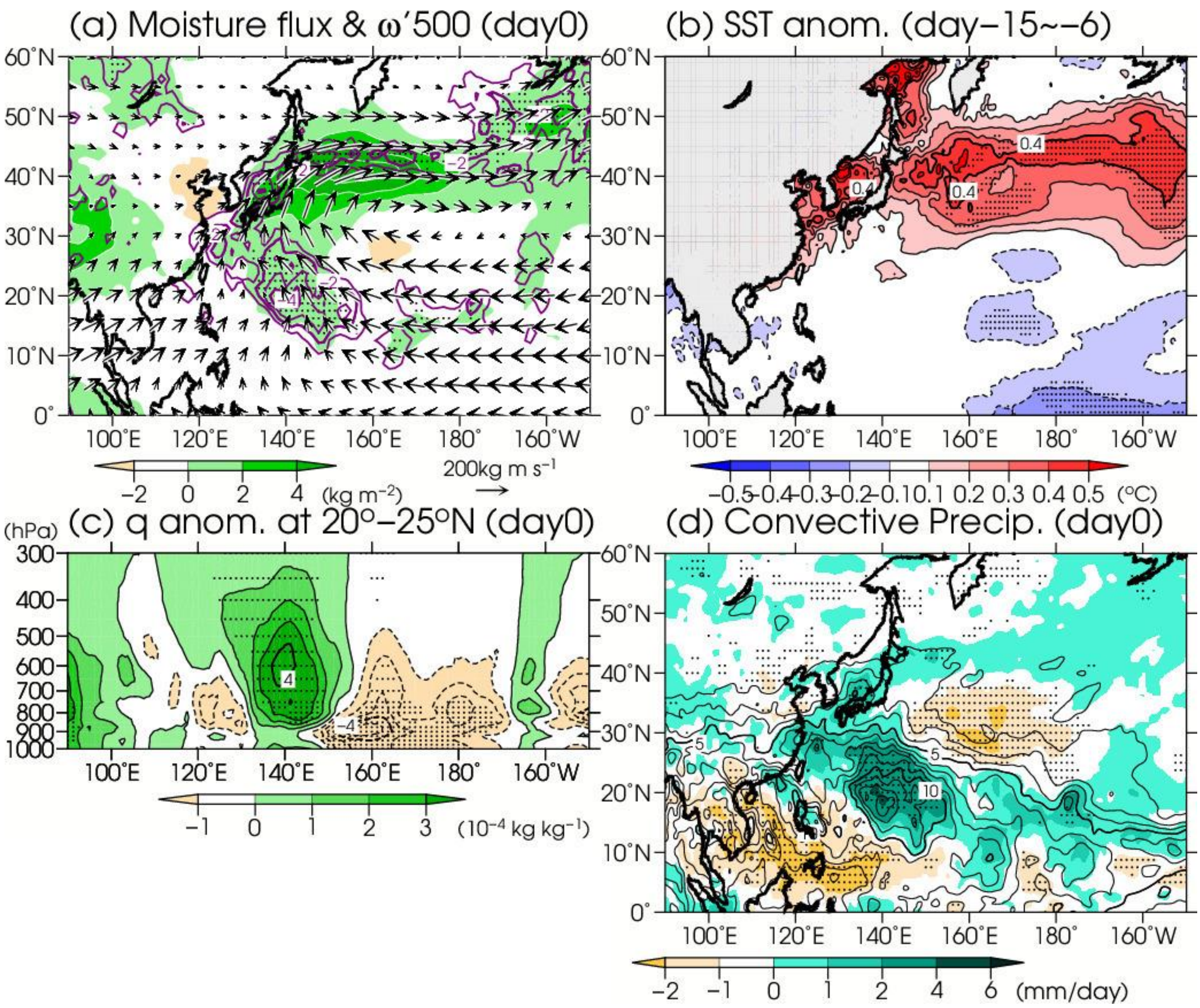

Fig. 12. Composite of 5-day averaged (a) vertically integrated moisture flux (vectors; unit: kg m s^{-1}), anomalous specific humidity (shading; unit: kg m^{-2}), anomalous 500-hPa negative vertical p-velocity (purple contour; interval: 1×10^{-2} Pa s^{-1}) on day 0, (b) anomalous SST (unit: ^{o}C) averaged from day -15 to day -6, (c) longitude-height cross section of anomalous specific humidity (unit: 10^{-4} kg kg^{-1}) averaged between 20^{o}N and 25^{o}N on day 0, and (d) convective precipitation (contour; unit: mm day^{-1}) and the anomalies (shading) on day 0. The vertical integration in (a) is taken from 1000 hPa to 500 hPa. In (d), the contour is shown over the region where the precipitation exceeds 2

mm day^{-1} at the interval of 1 mm day^{-1}. Dots indicate statistical significance at a 95% confidence level of the anomalous (a) negative vertical p-velocity, (b) SST, (c) specific humidity, and (d) convective precipitation.

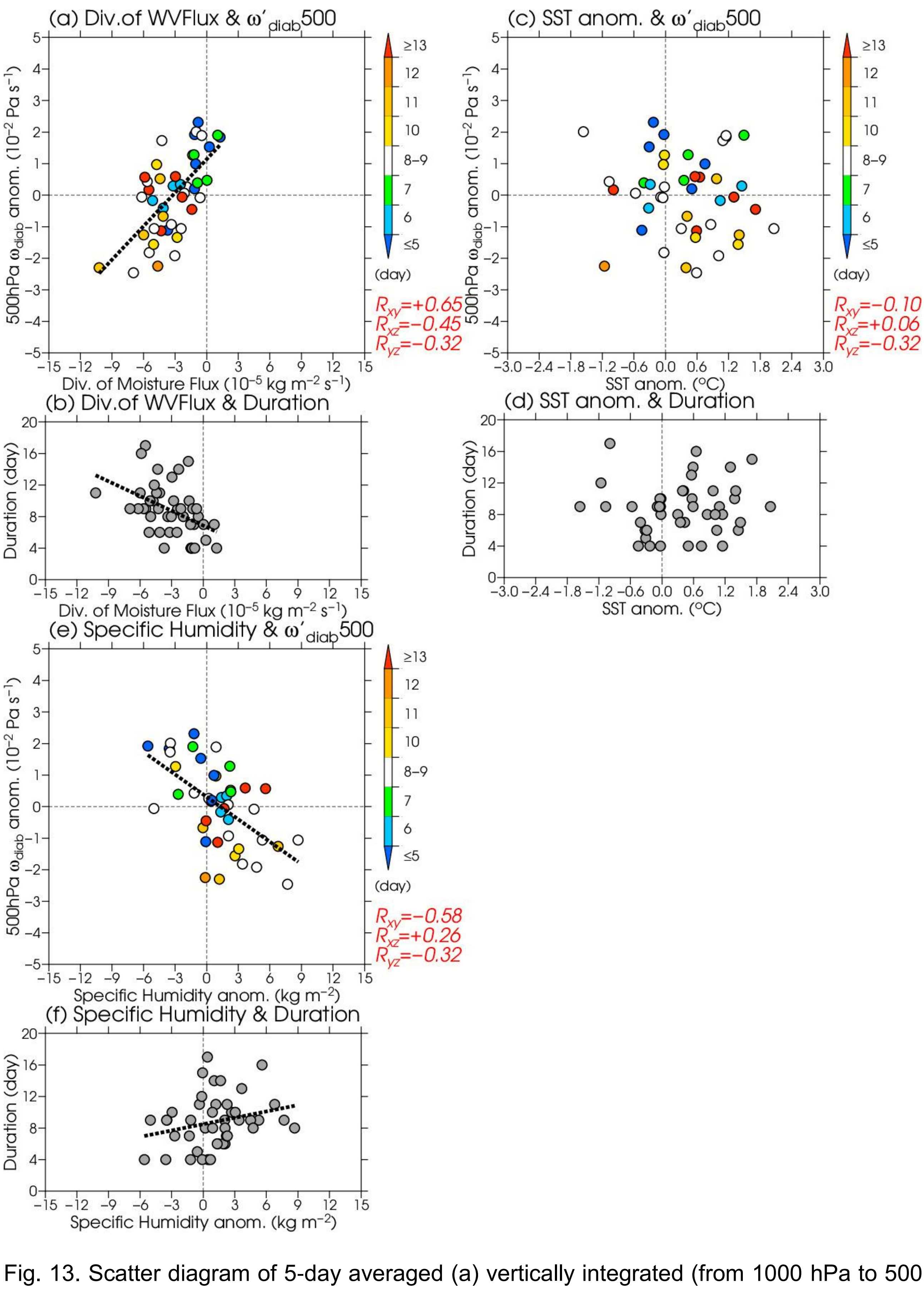

Fig. 13. Scatter diagram of 5-day averaged (a) vertically integrated (from 1000 hPa to 500 hPa) moisture flux divergence (X-axis; unit: 10^{-5} kg m^{-2} s^{-1}) on day 0 averaged over

region A (Fig. 1b), (c) anomalous SST (X-axis; unit: °C) averaged from day -15 to day -6 over region B (Fig. 1b), (e) vertically integrated (from 850 hPa to 500 hPa) anomalous specific humidity (X-axis; unit: kg m^{-2}) on day -2 averaged over region C (Fig. 1b), and diabatic component of 500-hPa anomalous vertical p-velocity (ω'_{diab}; Y-axis; unit: 10^{-2} Pa s^{-1}) on day 0 averaged over region A for the 44 RWB cases. (b), (d), and (f) are same as (a), (c), and (e), but the Y-axis denotes the duration. Dashed lines denote regression lines of Y- on X-components, with a confidence level of the correlation coefficients between the two components greater than 90%. Colors in (a), (c), and (e) represent the duration, which is referred to as Z-component. The corresponding correlation coefficients between X- and Y-components (R_{xy}), X- and Z-components (R_{xz}), Y- and Z-components (R_{yz}) are shown at the lower right of (a), (c), and (e).

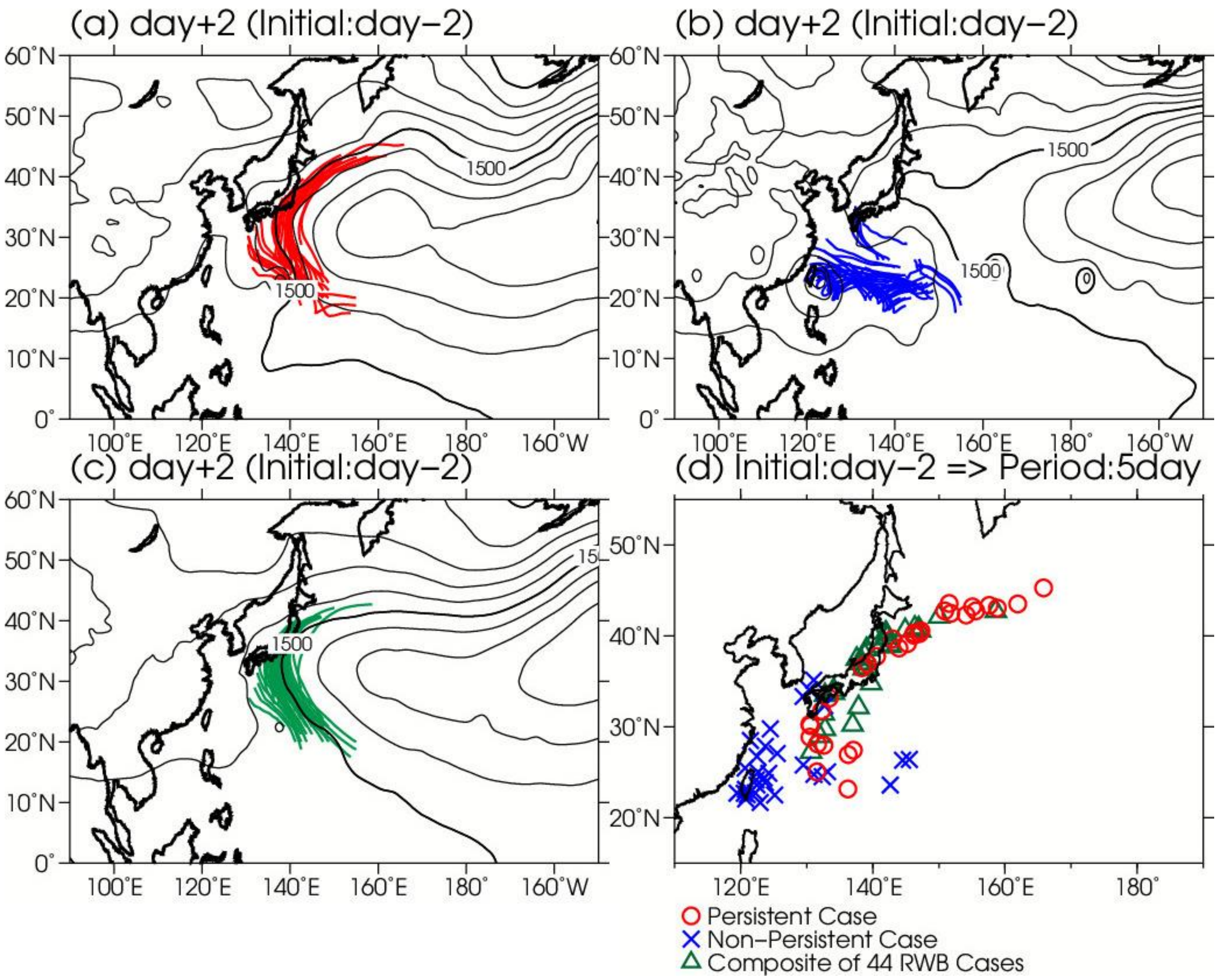

Fig. 14. Forward trajectories initialized from 00 UTC on day -2 until 18 UTC on day +2, for (a) the persistent case (red lines), (b) the non-persistent case (blue lines), and (c) the composite of the 44 RWB cases (green lines). The passive tracers originate from the subtropical WNP east of the Philippines, where the composite of 500-hPa anomalous vertical p-velocity is significant at a confidence level of 95% on day -2. Contours in (a, b, c) denote 850-hPa height (unit: m) in each case with the intervals of 20 m. Red circles, blue crosses, and green triangles in (d) indicate positions of the advected tracers at 18 UTC on day +2 for the persistent and non-persistent cases, and the composite, respectively.

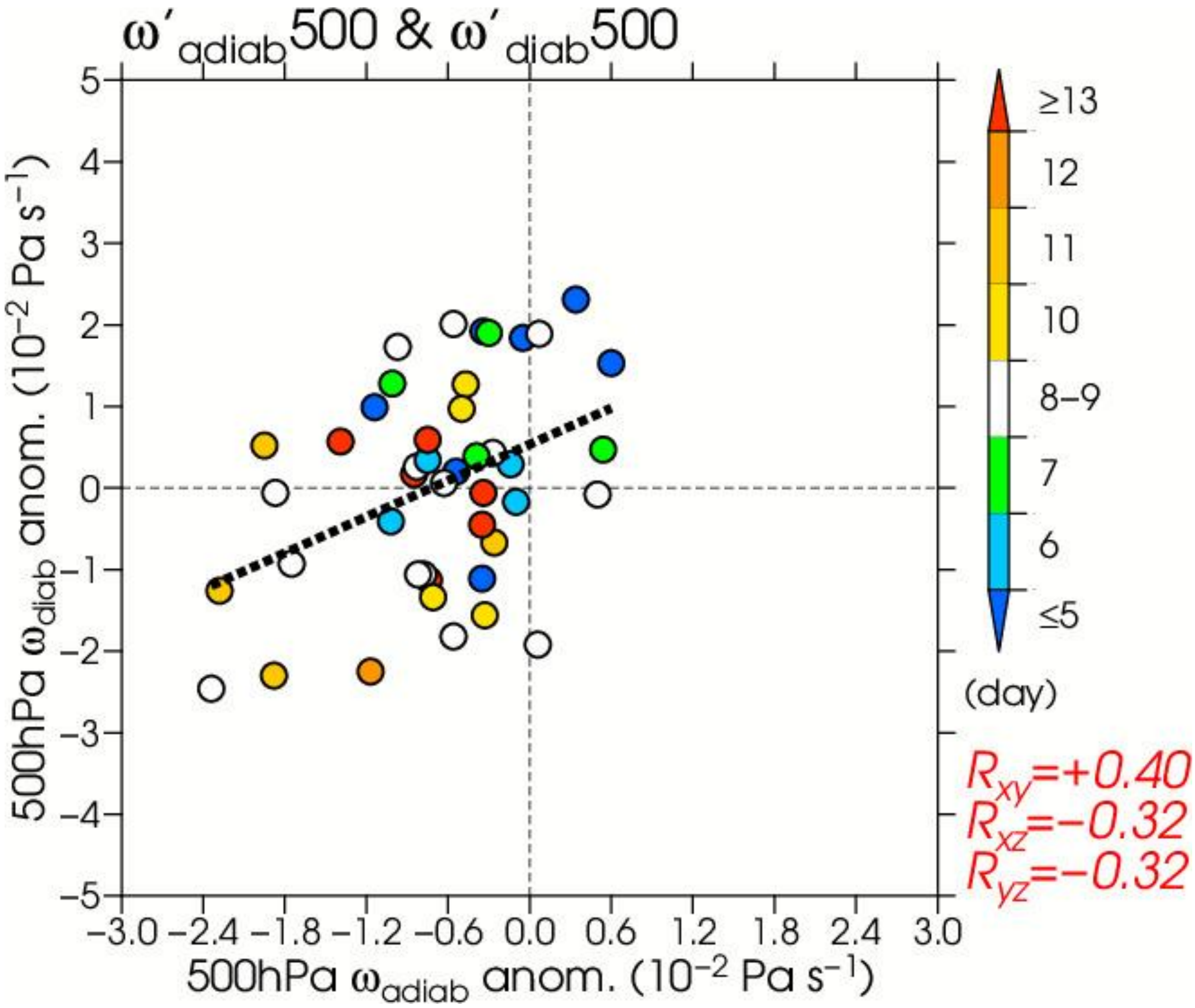

Fig. 15. Same as Fig. 13, but for 500-hPa anomalous vertical p-velocity by the adiabatic component (ω'_{adiab}; X-axis; unit: 10^{-2} Pa s^{-1}) and that by the diabatic component (ω'_{diab}; Y-axis) averaged over region A on day 0.

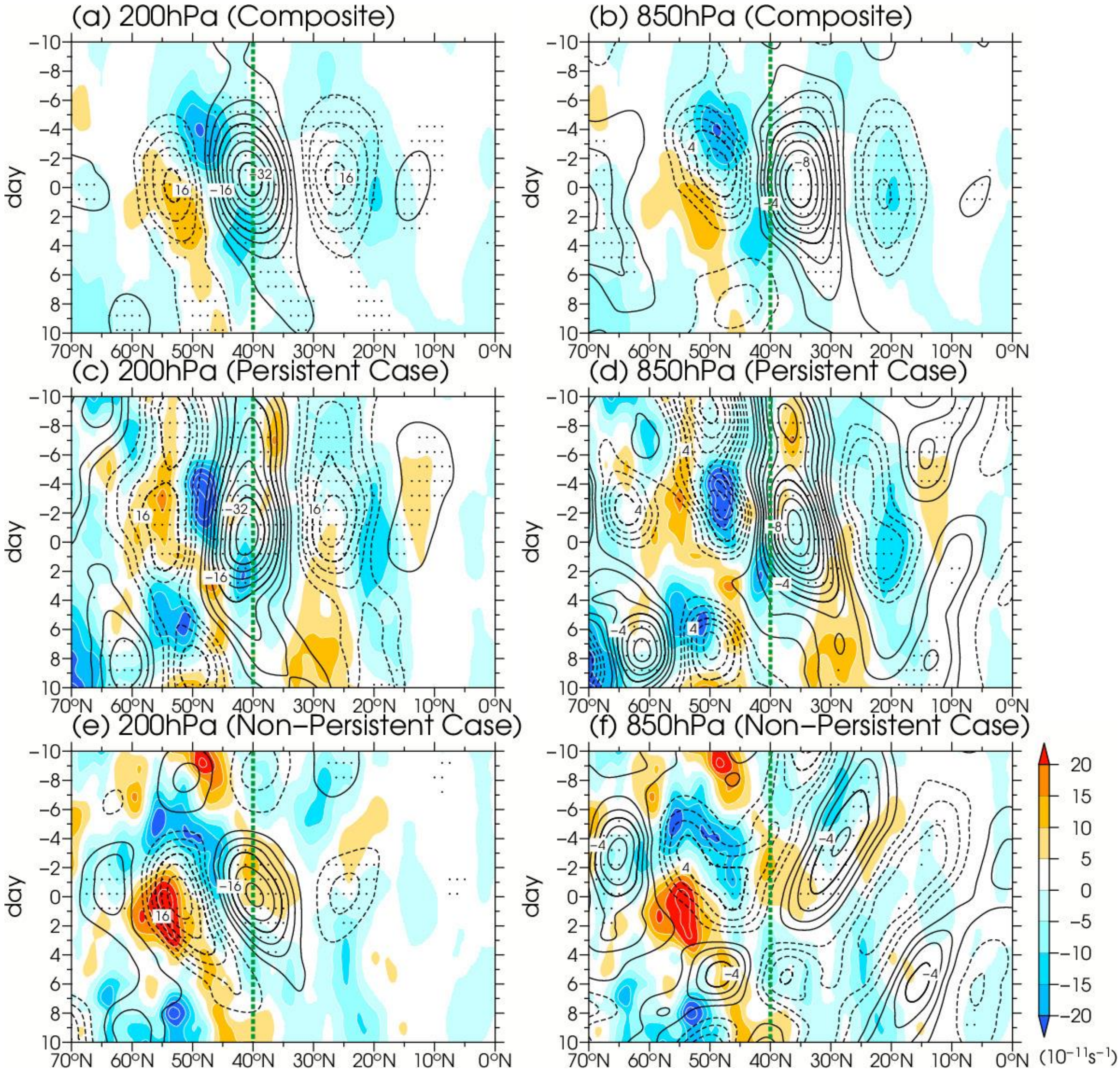

Fig. 16. Same as Fig. 7, but shadings indicate 200-hPa anomalous absolute vorticity tendency associated with vortex stretching (unit: 10^{-11} s^{-2}) averaged between 130°E and 160°E.

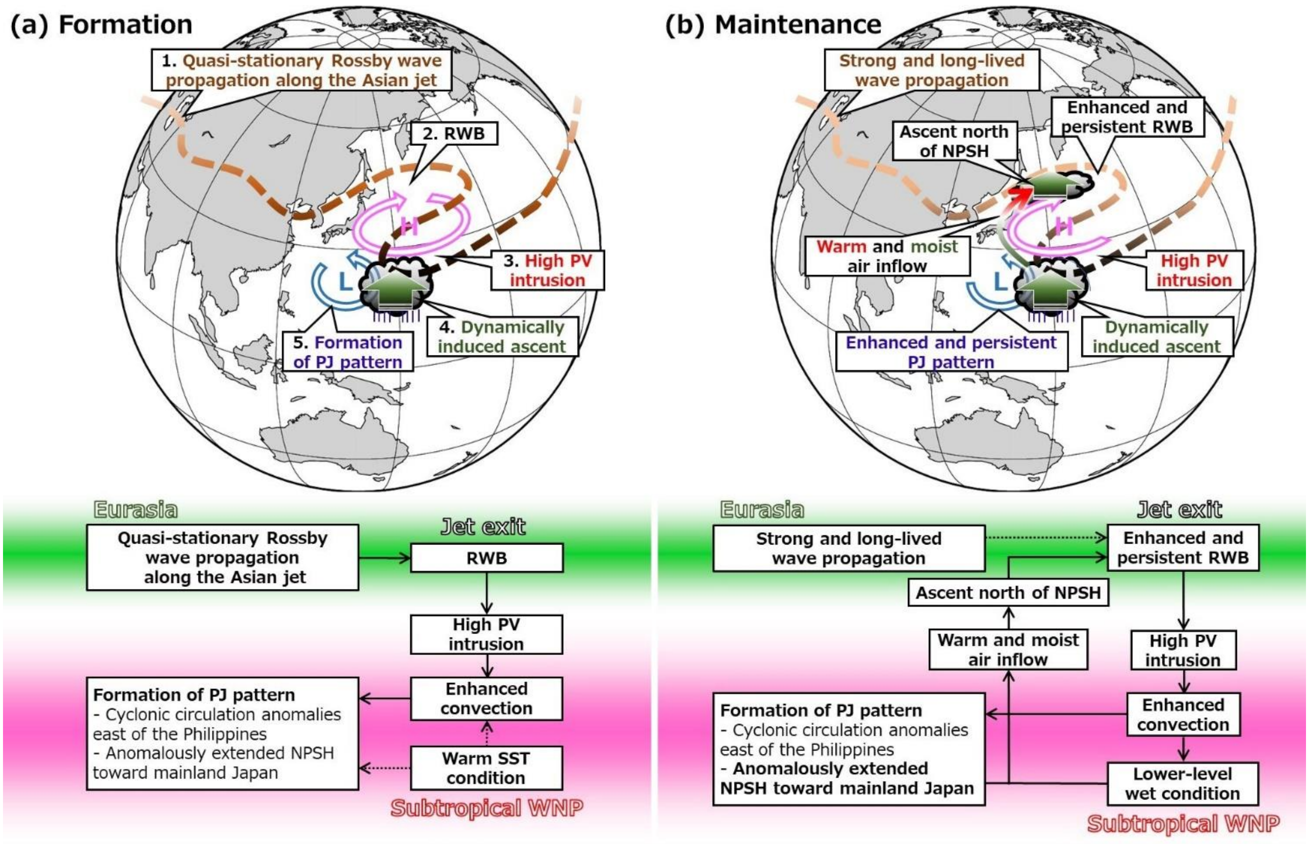

Fig. 17. A schematic diagram describing (a) the linking mechanism of the quasi-stationary Rossby wave propagation along the Asian jet and the PJ pattern through the RWB east of Japan shown in Takemura and Mukougawa (2020), and (b) the maintenance mechanism of the once triggered RWB and PJ pattern shown in this study. (a) and (b) is according to the results of lag composite analysis for the 44 RWB cases (Takemura and Mukougawa 2020) and that for the persistent case (Fig. 3), respectively. Brown-colored dashed lines denote the subtropical jet stream including the Asian jet. “L” and “H” indicate centers of the cyclonic and anticyclonic circulation anomalies in the lower troposphere associated with the PJ pattern, respectively. Green–red-colored curved arrow in (b) indicates the anomalous warm and moist air inflow along the fringe of anomalously extended NPSH (“H”). Green-colored bold straight arrows indicate

anomalous ascent resulting from (a, b) the high PV intrusion toward the subtropical WNP, and (b) the anomalous warm and moist air inflow.